PERIODICA POLYTECHNICA
TRANSPORTATION ENGINEERING

TECHNICAL UNIVERSITY OF BUDAPEST

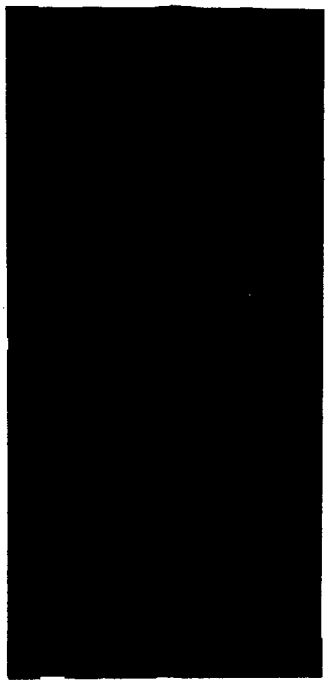

Vol. 24. No. 1.
1996

PERIODICA POLYTECHNICA

A contribution to international technical sciences, published by the Technical University of Budapest in six separate series, covering the following sciences:

Chemical Engineering
Civil Engineering
Electrical Engineering and Informatics
Mechanical Engineering
Social and Management Sciences (Earlier: Humanities and Social Sciences)
Transportation Engineering

TRANSPORTATION ENGINEERING SERIES

Published twice a year

Contributions in transportation engineering should be sent to the address of the journal:

TECHNICAL UNIVERSITY OF BUDAPEST
Periodica Polytechnica
Transportation Engineering
H-1521 Budapest, HUNGARY
Telefax: + 36 1 463-3041

For subscriptions please contact "Andreas Hess" Ltd. (Mail: P.O.B. 290, Budapest III, H–1300; Telefax: +36 1 250–2188) or its representatives abroad.

Exchange copies should be requested from the International Exchange Department of the Central Library of the Technical University of Budapest
(H–1111 Budapest, Budafoki út 4.; Telefax: + 36 1 463–2440).

Published by the Technical University of Budapest, Hungary.

HU ISSN: 0303–7800

PERIODICA POLYTECHNICA

TRANSPORTATION ENGINEERING

Vol. 24 * No. 1 * 1996

TECHNICAL UNIVERSITY
BUDAPEST

PRINTED IN HUNGARY
LIGATURA LTD – ÁFÉSZ PRESS, VÁC

PERIODICA POLYTECHNICA SER. TRANSP. ENG. VOL. 24, NO. 1, PP. 3-17 (1996)

THEORY OF ANOMALIES AND ITS APPLICATION TO AIRCRAFT CONTROL

József ROHÁCS

Department of Aircraft and Ships
Technical University of Budapest
H-1521 Budapest, Hungary

Received: November 19–22, 1994

Abstract

The anomalies are deviations in the system parameters or service characteristics initiating the changes in the technical and operational characteristics and finally generate decreasing of the prescribed or designed working quality of system.

The general lecture deals with the basic elements of the theory of system anomalies, describes the mean problems of theory and shows the recommended models for valuation of anomalies effects on system characteristics. The system anomalies play an important role in accuracy and dynamics of control systems. In many cases they can be modelled as the additive errors in the output characteristics (motion variables) measured and used as feedback signals. Some specific problems of application of system anomalies theory to the aircraft control systems are discussed in the second part of the paper.

Keywords: aircraft control systems, system anomalies.

1. Introduction

The parameters of the large systems like aircraft are scattering near their prescribed nominal levels. During operation of the systems these deviations in the characteristics are changing stochastically, mostly in cumulative way. According to our experiences gained in practice, the system parameter deviations [1, 2] can achieve 4 – 10% relatively to their nominal levels.

The system parameter deviations involve the changes in aerodynamic characteristics, performance data and characteristics of stability and controllability. The deviations in the system parameters are greater then which could be obtained by normal control methods which do not generate the failures or standstills of given systems can be called system anomalies. The investigation of these parameter deviations and their effects on system characteristics is an actual new theoretical and practical problem.

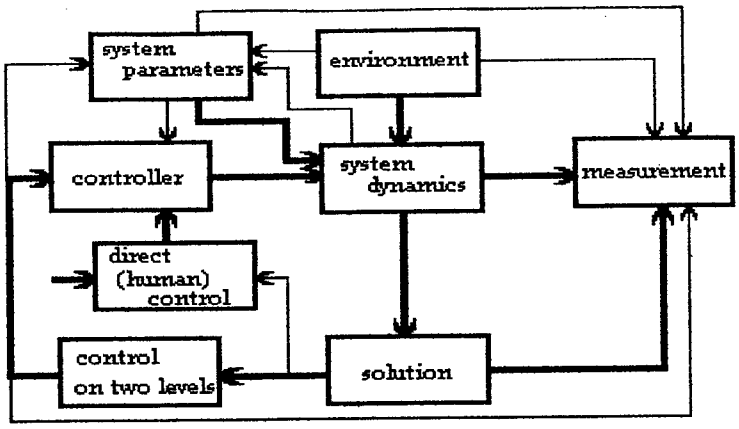

Fig. 1. Representation of system control

2. System Anomalies

The system can be given by its system parameters. The parameters describing the structure and geometrical characteristics can be called as constructional parameters. The parameters representing the operational process of the given system are the operational parameters.

The parameters of large systems, i.e. real constructional-technical characteristics of aircraft and its systems are scattered to a great extent in the neighbourhood of the rated values prescribed in technical documentation. During the operation the deviations mentioned above continue to increase stochastically mostly in a cumulative way as a function of [1, 2]:

- the physical-technical peculiarities of the structural material applied,
- the peculiarities of their design and manufacture,
- the technical and economical condition of operation, and
- the intensity of operation.

These deviations in parameters can be divided into three parts [3]:

- the parameter uncertainties, which can be obtained by some specific methods of control, i.e. robust control,
- the anomalies, which are greater deviations than uncertainties but they do not generate the failures or standstill of systems,
- errors, namely deviations in characteristics coming out of their prescribed tolerance zones and generating the failures and standstills of systems.

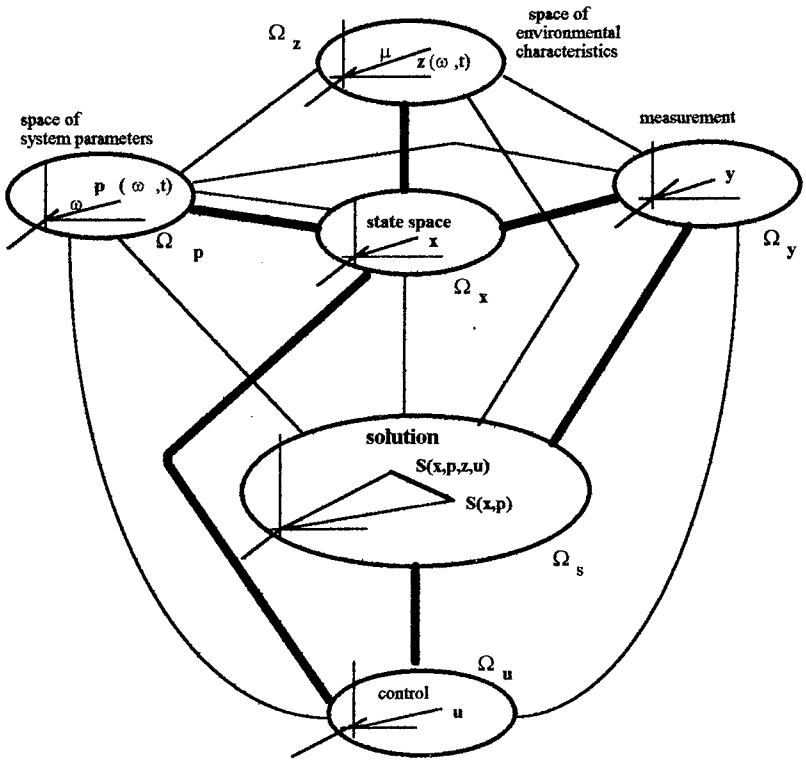

Fig. 2. Aircraft control in general case

Generally, the errors are investigated by reliability theory and risk analysis very well [4, 5]. The small disturbance in parameters, e.g. parameter uncertainties, are investigated very well, too [6]. The robust control gives possibilities to manage with uncertainties. But the influences of system parameter anomalies on the system characteristics have not been studied yet on the level needed. The investigation of the aircraft system parameter anomalies on real flight situations, on risk of flight operation and on the control quality is one of the most actual problem of aeronautical sciences.

The changes in the system parameters naturally involve also the changes in system characteristics, in our case the deviations in aerodynamic, flight engineering and flight safety characteristics. Therefore these anomalies and their effects on the system characteristics should be investigated in details. For this aim we recommend to develop the system anomalies theory.

The theory of anomalies deals with system anomalies and their effects on the system dynamics. It should determine the methods of description

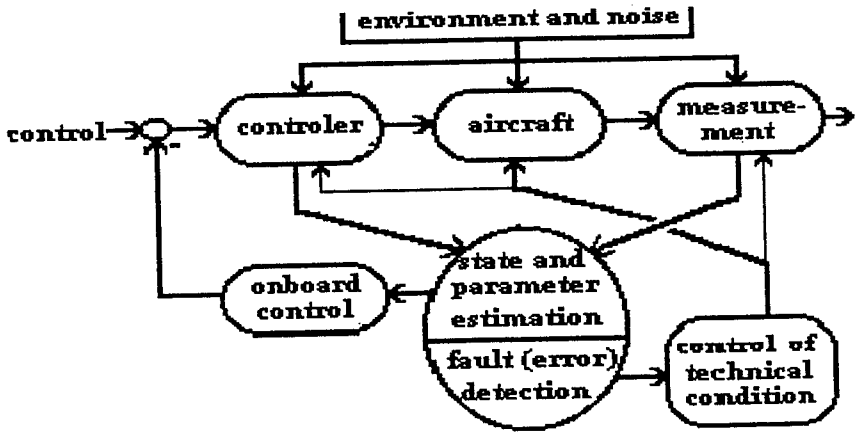

Fig. 3. System anomalies control

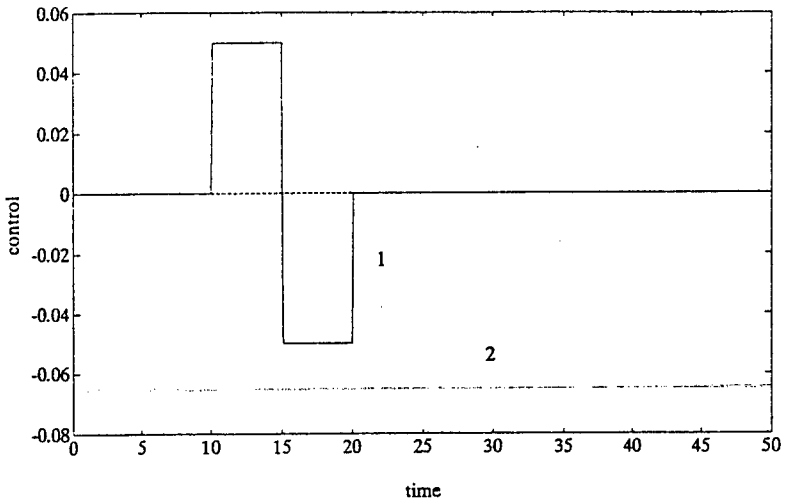

Fig. 4. Aileron deflection input (1) and the modelled anomaly in the rolling moment (2)

of anomalies, the mean tasks of theory and the methods of solving the problems.

Generally, the deviations in the structural, operational and service characteristics can reach and even exceed the tolerance limits essentially in three different ways [3]. In first case the system anomalies take place

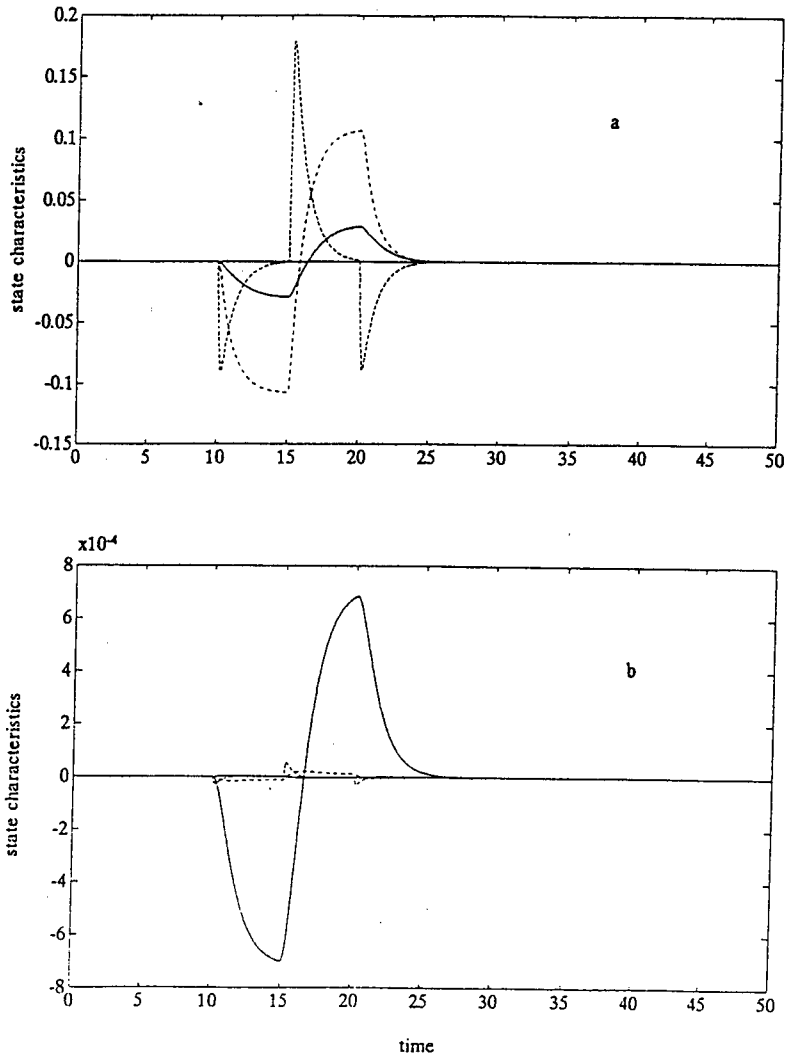

Fig. 5. The response of the system with a simple feedback (a) and the system with the robust feedback controller (b) on the aileron deflection input. (— slideslip angle, – – – roll rate, ··· yaw rate, – · –· roll angle)

under influence of sudden loads greater than which was taken into account during design. In second case characteristics are changing gradually and reaching the tolerance range in a predictable way. In the third case the tolerance range becomes restricted for some other reason, e.g. by effect of other anomalies or errors, and the excess of the tolerance range can occur

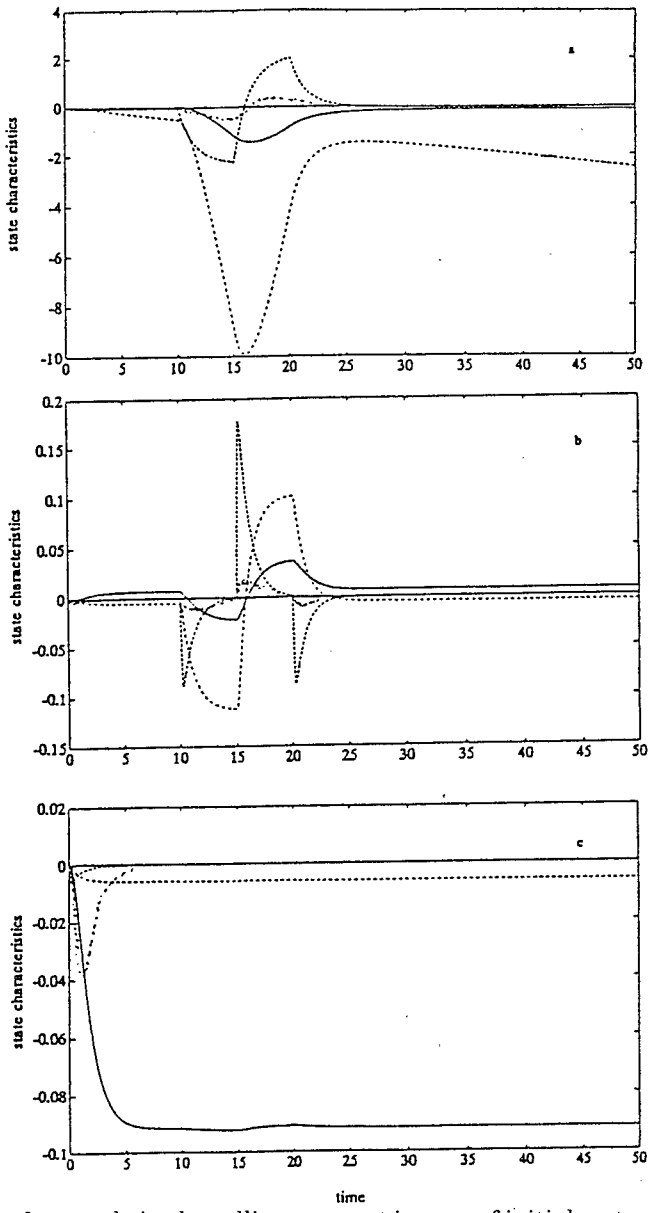

Fig. 6. Effect of anomaly in the rolling moment in case of initial system (a), system with simple feedback (b) and system with robust feedback controller (c). (— slideslip angle, – – – roll rate, ··· yaw rate, – · –· roll angle)

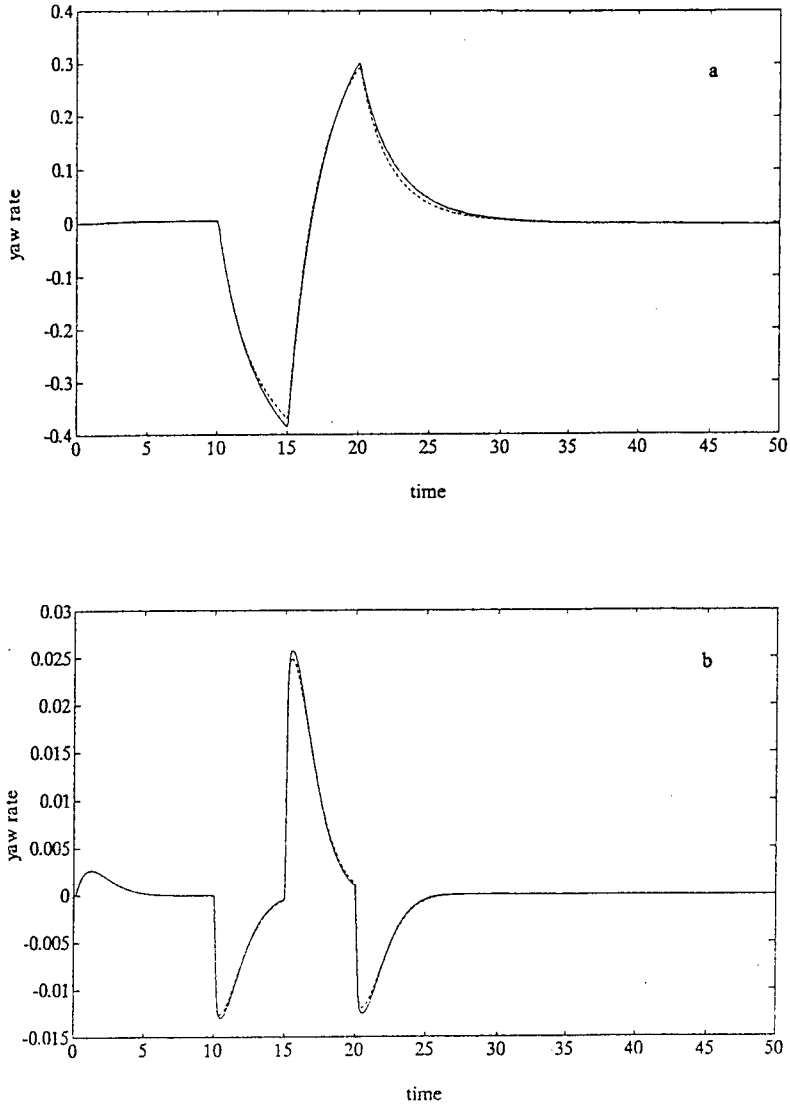

Fig. 7. The effect of decreasing in state matrix element $\mathbf{A}(2,2)$ of initial system with simple feedback (a), and system with robust feedback controller (b) on the response in case of aileron deflection only

even under the influence of otherwise normal design loads.

The system anomalies formed in the described way can be called as sudden, gradual (or parametric) and relaxation anomalies. Consequently, the probability of the dwelling of the characteristics within the tolerance

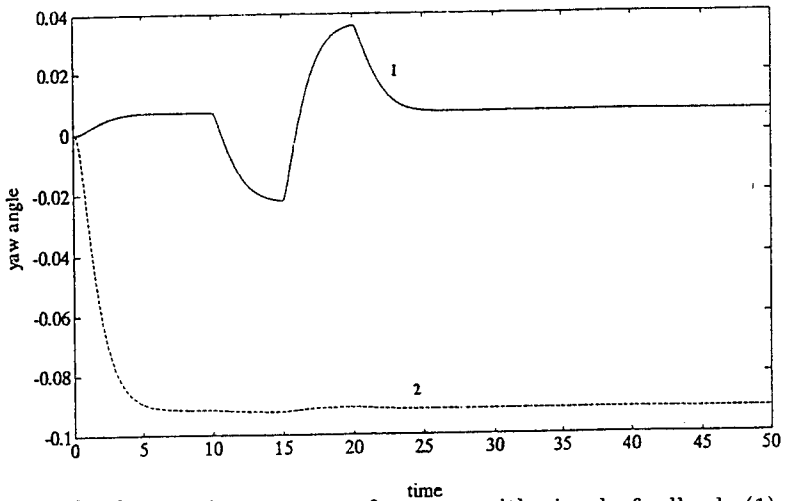

Fig. 8. Yaw angle changes in response of system with simple feedback (1) and system with robust feedback controller (2) in case of system anomaly in rolling moment

range can be given according reliability theory with the help of exponential, normal and two-parameter exponential laws.

On the other hand the system anomalies can be classified as multiplicative (β_1), delay-time (β_2) and additive (β_3) deviations in the parameters and they can be taken into account in the mathematical normalisation by following way:

$$\mathbf{p} = (1 + \beta_1)\mathbf{p}_n(t - \beta_2) + \beta_3 \,, \tag{1}$$

where $\mathbf{p}_n$ is the initial (nominal) values vector of parameters and the random coefficients β depend on the realised control and real operational situations (flight situations).

3. General Model

When examining the dynamics or technical condition of complicated systems like aircraft, it seems to be describable easily for an engineer if the variation of its state vector $\mathbf{x}$ chosen appropriately is expressed as follows

$$\dot{\mathbf{x}} = \mathbf{F}(\mathbf{x}, \mathbf{u}, t) \,, \tag{2}$$

where $\mathbf{u}$ is a control vector.

In reality the controlled dynamics of the systems can be investigated on the basis of much more complicated picture shown on *Fig. 1.*

In fact, the variation of state vector $\mathbf{x}$ is influenced by the variation in the instantaneous values of a number of factors (service conditions, methods of maintenance and repair applied, the realised management, the characteristics of the flight, the atmospheric conditions, etc.). These influences can be given in terms of stochastic processes, random variables or random space (turbulence of atmosphere). Moreover, state vector $\mathbf{x}$ cannot generally be measured directly. Instead, some output signal vector $\mathbf{y}$ can be measured. Consequently, the controlled motion of the aircraft or their technical conditions, their dynamics can be described only by a much more complicated model than in (2), namely by the following general set of stochastic differential equations [3]:

$$\begin{aligned}
\mathrm{d}\mathbf{x} &= f_x[\mathbf{x}(t), \mathbf{x}(t-\tau_x), \mathbf{p}(\mathbf{x},\mathbf{z},\omega,\mu,t), \mathbf{z}(\mu,t), \mathbf{u}(t), \omega, \mu, t]\mathrm{d}t + \\
&\quad + \sigma_x(\mathbf{x},\mathbf{p},\mathbf{z},\omega,\mu,t)\mathrm{d}W, \\
\mathbf{y} &= f_y[\mathbf{x}(t), \mathbf{x}(t-\tau_y), \mathbf{p}(\mathbf{x},\mathbf{z},\omega,\mu,t), \mathbf{z}(\mu,t), \mathbf{u}(t), \omega, \mu, t] + \\
&\quad + \sigma_y(\mathbf{x},\mathbf{p},\mathbf{z},\omega,\mu,t)\xi\,, \qquad (3) \\
\mathbf{u}(t) &= f_u[\mathbf{x}(t), \mathbf{x}(t-\tau_u), \mathbf{p}(\mathbf{x},\mathbf{y},\omega,\mu,t), \mathbf{z}(\mu,t), \mathbf{u}(t), \omega, \mu, t]\,, \\
\mathbf{x}(t=t_0) &= \mathbf{x}_0(t=t_0,\omega_0,\mu_0)\,, \\
\mathbf{y}(t=t_0) &= \mathbf{y}_0(t=t_0,\omega_0,\mu_0)\,;
\end{aligned}$$

where $\mathbf{x} \in R^n$ is the state vector, $\mathbf{p} \in R^k$ is the parameter vector characterising the state of the aircraft, $\mathbf{z} \in R^1$ is the vector of environmental characteristics (vector of service conditions), $\mathbf{u} \in R^m$ is the input (control) vector, $\mathbf{y} \in R^r$ is the output (measurable) signal vector $\mathbf{W} \in R^s$ and $\xi \in R^q$ are the noise vectors (in simplified case the Wiener and Gaussian noise vectors, respectively), σ_x, σ_y are the noise transfer matrices, ω and μ are the random variables assigning the position of vectors $\mathbf{p}$ and $\mathbf{z}$ within admissible space Ω_p Ω_z described by density functions $f_p(\cdot)$, $f_z(\cdot)$, t is the time, and τ_x, τ_y, τ_u are the time-delay vectors.

In general case, the aim of aircraft operation is to use the aircraft for their primary purposes (transport the passengers) to maximum time with minimum specific (related to the unit time of operation) life-cycle-cost at prescribed level of safety and reliability. It can be seen that the knowledge of the changes in the operational and structural characteristics is indispensably required for controlling the service and operational process of this kind.

The realising of this kind of aircraft control can be based on the principle shown on *Fig. 2.* The system parameters $\mathbf{p}$ are changing under the real environmental conditions $\mathbf{z}$ real flight situation and technical works, e.g. control $\mathbf{u}$ realised on aircraft and generate the given realisation of state vector $\mathbf{x}$. The state realisations, of course, depend on the system parameters and real environmental conditions, too. The measurable input vector $\mathbf{y}$ depends on these system parameter deviations, real environmental conditions and real state change realisations. As it can be understood, the real system parameter, environmental characteristic and state vectors are mapped

by solution on the solution space into $\mathbf{S}(\mathbf{x}, \mathbf{p}, \mathbf{z}, \mathbf{u})$. From the other hand the system parameters and states can be estimated on basis of measured $\mathbf{y}$. (The difference in the solution guided by real processes and result of identification can generate the systematic anomalies in the constructed system.) The estimated solution $\acute{\mathbf{S}}(\mathbf{x}, \mathbf{p})$ should be applied [7] to synthesis of control $\mathbf{u}$ having the two levels. The first is the operative control or state control (real control on the board) and the second is control of system parameter deviations (technical maintenance and repair include the regulation of system parameters). Connection between these two levels should be realised through the fault and failure detection.

Set of *Eq.* (3) can be given also in a very simplified time-invariant linearized uncertain system form

$$\begin{aligned} \dot{\mathbf{x}}(t) &= \mathbf{A}(\omega,t)\mathbf{x}(t) + \mathbf{B}(\omega,t)\mathbf{u}(t) + \mathbf{H}(\mu,t)\mathbf{z}(t) + \\ &\quad + \mathbf{A}_{nx}(\mathbf{x},\mathbf{u},\omega,t) + \mathbf{G}_x(\nu,t)\eta(t)\,, \\ \mathbf{y}(t) &= \mathbf{C}(\omega,t)\mathbf{x}(t) + \mathbf{D}(\omega,t)\mathbf{u}(t) + \mathbf{G}_y(\nu,t)\xi(t) + \mathbf{A}_{ny}(\mathbf{x},\mathbf{u},\omega,t)\,, \end{aligned} \tag{4}$$

where $\mathbf{A}$, $\mathbf{B}$, $\mathbf{H}$, $\mathbf{C}$ and $\mathbf{D}$ are the state, control, environmental, output and input influence matrices of $n \times n$, $n \times m$, $n \times l$, $r \times m$ and $r \times m$ dimensions, respectively, $\mathbf{G}_x$, $\mathbf{G}_y$ are the noise transfer matrices, η and ξ are the noise vectors, ω and ν are the random values determining the deviations in the matrix elements. The stochastic time-varying vectors $\mathbf{A}_{nx}$, $\mathbf{A}_{ny}$ include the effects of system anomalies depending on the real flight situations initiated by realised control.

In a simple case, for the first approximation the linearized model with system anomalies can be given in following form:

$$\begin{aligned} \dot{\mathbf{x}}(t) &= \mathbf{A}(\omega,t)\mathbf{x}(t) + \mathbf{B}(\omega,t)\mathbf{u}(t) + \mathbf{A}_{nx}(\omega,t)\,, \\ \mathbf{y}(t) &= \mathbf{C}(\omega,t)\mathbf{x}(t)\,. \end{aligned} \tag{5}$$

4. Description of the System Anomalies Effects

In consideration of types of anomalies described in part titled system anomalies, the general model in simplified case can be rewritten in form of multivariable perturbed linear system with time-delay and additive system anomalies:

$$\begin{aligned} \dot{\mathbf{x}}(t) &= (\mathbf{A} + \Delta A)\mathbf{x}(t) + (\mathbf{A}_d + \Delta\mathbf{A}_d)\mathbf{x}(t - \tau_d) + \mathbf{A}_n + (\mathbf{B} + \Delta\mathbf{B})\mathbf{u}(t)\,, \\ \mathbf{y}(t) &= (\mathbf{C} + \Delta\mathbf{C})\mathbf{x}(t) + (\mathbf{D} + \Delta\mathbf{D})\mathbf{u}(t) + \mathbf{H}_m\,, \end{aligned} \tag{6}$$

where the $\Delta\mathbf{A}$, $\Delta\mathbf{A}_d$, $\mathbf{A}_n$, $\Delta\mathbf{B}$, $\Delta\mathbf{C}$, $\Delta\mathbf{D}$ and $\mathbf{H}_m$ represent the uncertainties and anomalies.

In set of *Eqs* (6) the $\Delta\mathbf{A}$, $\Delta\mathbf{A}_d$, $\Delta\mathbf{B}$, $\Delta\mathbf{C}$ and $\Delta\mathbf{D}$ contain the changes in the partial derivatives of vector functions f_x and f_y of model (3) respectively to state and control vector elements. So, they take into account the changes in gradient of these functions only. They are the multiplicative anomalies.

The $\mathbf{A}_n$ and $\mathbf{H}_m$ are the additive anomalies in the state and measurement characteristics.

The effects of the system anomalies can be given by the following type of probabilities [1]:

$$\begin{aligned} &P_1\{\mathbf{y}(t) \in \Omega_y | t_0 \le t \le t_0 + \tau\,,\ \mathbf{x} \in \Omega_x,\ \mathbf{u} \in \Omega_u,\ \mathbf{z} \in \Omega_z,\ \mathbf{p} \in \Omega_p\}\,, \\ &P_2\{\mathbf{u}(t) \in \Omega_u | t_0 \le t \le t_0 + \tau\,, \mathbf{x} \in \Omega_x,\ \mathbf{z} \in \Omega_z,\ \mathbf{p} \in \Omega_p,\ \mathbf{y} \in \Omega_y\}\,; \end{aligned} \tag{7}$$

where the admissible vectorial fields of characteristics are given by Ω.

If joint density function

$$f_\Sigma = f[\mathbf{x}(t), \mathbf{u}(t), \mathbf{z}(t), \mathbf{p}(t), \mathbf{y}(t)] \tag{8}$$

is known, then the recommended characteristics (7) can be calculated as follows:

$$\begin{aligned} P_1\{\mathbf{y}(t) \in \Omega_y | \ldots\} &= \frac{\int\limits_{\Omega_i} f_\Sigma \,\mathrm{d}\mathbf{x}\,\mathrm{d}\mathbf{u}\,\mathrm{d}\mathbf{z}\,\mathrm{d}\mathbf{p}\,\mathrm{d}\mathbf{y}}{\int\limits_{-\infty}^{+\infty} \mathrm{d}\mathbf{y} \int\limits_{\Omega_j} f_\Sigma \,\mathrm{d}\mathbf{x}\,\mathrm{d}\mathbf{u}\,\mathrm{d}\mathbf{z}\,\mathrm{d}\mathbf{p}} \quad \begin{matrix}(i \in \mathbf{x}, \mathbf{u}, \mathbf{z}, \mathbf{p}, \mathbf{y}) \\ (j \in \mathbf{x}, \mathbf{u}, \mathbf{z}, \mathbf{p})\end{matrix} \\ P_2\{\mathbf{u}(t) \in \Omega_u | \ldots\} &= \frac{\int\limits_{\Omega_i} f_\Sigma \,\mathrm{d}\mathbf{x}\,\mathrm{d}\mathbf{u}\,\mathrm{d}\mathbf{z}\,\mathrm{d}\mathbf{p}\,\mathrm{d}\mathbf{y}}{\int\limits_{-\infty}^{+\infty} \mathrm{d}\mathbf{u} \int\limits_{\Omega_j} f_\Sigma \,\mathrm{d}\mathbf{x}\,\mathrm{d}\mathbf{z}\,\mathrm{d}\mathbf{p}\,\mathrm{d}\mathbf{y}} \quad \begin{matrix}(i \in \mathbf{x}, \mathbf{u}, \mathbf{z}, \mathbf{p}, \mathbf{y}) \\ (j \in \mathbf{x}, \mathbf{z}, \mathbf{p}, \mathbf{y})\end{matrix} \end{aligned} \tag{9}$$

5. Problems and Control of System Anomalies

The problems of theory of system anomalies can be classified as the mean tasks of given theory:

- initial task – investigation of the structural and operational characteristics, signalization of the anomalies and the statistical description of the anomalies,
- direct task – study the effects of system parameter anomalies on the aerodynamics, flight mechanics, controllability and stability,

- inverse task (synthesis) – determining of the bounds for the system parameters from the given bounds (admissible field) of operational characteristics, e.g. flight safety, quality of manoeuvres, controllability,
- basic task – create the control for the system with anomalies,
- complementary task – determining the basic and additional information for solving the different problems connected with system anomalies, e.g. model- formation, optimal control, identification, etc.

The initial task can be solved by application of theory of measurement, statistics and stochastic approximation. The direct and the inverse tasks are based on the theory of flight and on using the sensitivity theory.

The basic task is the completely new task. The mean idea is the change of the goal of operation. The new goal is using the aircraft to maximum time with specific life cost expenditure under predefined service condition with keeping the system parameters in the prescribed tolerance zones. Therefore we should define the control of anomalies. The technical condition of aircraft can be controlled on two different levels [7]. At first, we can use the pilot or automatic control of aircraft in case if the motion characteristics are different from given values. In this case the control should be realised on the board of aircraft. Secondary, on the basis of state or parameter estimation results we can use some technical methods of operation (e.g. methods of maintenance or repair) for replacing the nominal system parameters. The connection between these two different levels of control is the fault or error detection (*Fig. 3*).

The complementary task should be solved through the application of the different theories like state and parameter estimation, theory of diagnosis, etc.

6. Control System Anomalies

We have a long period experience on the investigation of deviations in the structural (e.g. geometrical) characteristics of supersonic fighter and middle-size passenger aircraft [1, 2]. For example, we found the permanent deformation, e.g. permanent deviations in the geometrical characteristics of wings of fighters MiG-21 generated by micro motion of wing elements under big loads. The extent and form of these anomalies depend on the duty of the airplanes to be carried out, on the flying hours, on the circumstances of operation, on the technique of piloting the airplane (especially on the landing mode of operation), and on man's physiological characteristics. According to our experience the geometrical characteristic deviations of wings generate the changes in the zero-lift angles, relative cambers and asymmetry in the rolling direction.

These types of characteristic deviations generate the deviations in the aerodynamic characteristics and performance data and cause the problem in the flight stabilising, especially during flight test. The asymmetry in the deformations of right and left hand wings can be modelled as the additive errors in the measuring of the roll angle, $\Delta\phi_m$. This error in measurement is the element of the measurement anomalies vector $\mathbf{H}_m$.

In simple case, if the model can be written as follows

$$\begin{aligned} \dot{\mathbf{x}}(t) &= \mathbf{A}\mathbf{x}(t) + \mathbf{B}\mathbf{u}(t)\,, \\ \mathbf{y}(t) &= \mathbf{C}\mathbf{x}(t) + \mathbf{H}_m\,, \end{aligned} \tag{10}$$

and the control given as feedback control

$$\mathbf{u}(t) = -\mathbf{K}\mathbf{y}(t) = -\mathbf{K}(\mathbf{C}\mathbf{x}(t) + \mathbf{H}_m)\,, \tag{11}$$

then the close loop dynamics can be described by following equation:

$$\dot{\mathbf{x}}(t) = \mathbf{A}\mathbf{x}(t) - \mathbf{B}[\mathbf{K}(\mathbf{C}\mathbf{x}(t) + \mathbf{H}m)] = \mathbf{A}\mathbf{x}(t) - \mathbf{B}\mathbf{K}\mathbf{C}\mathbf{x}(t) - \mathbf{B}\mathbf{K}\mathbf{H}_m =$$

$$= (\mathbf{A} - \mathbf{B}\mathbf{K}\mathbf{C})\mathbf{x}(t) - \mathbf{B}\mathbf{K}\mathbf{H}_m\,. \tag{12}$$

Here the $\mathbf{B}\mathbf{K}\mathbf{H}_m$ represents the additive anomaly in state characteristics. So, the deviation in the structural characteristics can be modelled as the additive anomaly in the state characteristics or as the measurement error in the system input.

During our investigation of system anomalies, there were investigated different types of anomalies on the lateral feedback stabilising system. The nonlinearities and the time-delays are investigated very well in the theory of aerodynamics and flight mechanics. The nonlinearities should be taken into account only on the flight near the operational limits, for example at high angle of attack [8]. The third type of anomalies, the additive anomalies like rolling moment at zero roll angle caused by asymmetry in wing geometry could be more interesting for study.

There was investigated a lateral disturbed motion of the middle-size supersonic fighter at high subsonic speed equal to Mach number 0.9 flying on the altitude more than 10 km. The system of equation and the values of matrix elements were the following [9, 10]:

$$\begin{aligned} \dot{\mathbf{x}}(t) &= \mathbf{A}\mathbf{x}(t) + \mathbf{B}\mathbf{u}(t) + \mathbf{A}_n\,, \\ \mathbf{y}(t) &= \mathbf{C}\mathbf{x}(t) + \mathbf{D}\mathbf{u}(t)\,, \end{aligned}$$

$$\mathbf{x} = \begin{bmatrix} \beta &= \text{slideslip angle} \\ p &= \text{roll rate} \\ r &= \text{yaw rate} \\ \phi &= \text{roll angle} \\ \psi &= \text{yaw angle} \end{bmatrix}, \quad \mathbf{u} = -\begin{bmatrix} \delta_a &= \text{aileron deflection} \\ \delta_r &= \text{rudder deflection} \end{bmatrix},$$

$$\mathbf{A} = \begin{bmatrix} -98 & 0 & -0.995 & 0.35 & 0 \\ -18.9 & -1.23 & 1.6 & 0 & 0 \\ 2.79 & -0.3 & -0.263 & 0 & 0 \\ 0 & 1 & 0 & 0 & 0 \\ 0 & 0 & 1 & 0 & 0 \end{bmatrix}, \quad \mathbf{B} = \begin{bmatrix} 0 & 0.185 \\ -34.7 & 5.07 \\ -3.85 & -1.44 \\ 0 & 0 \\ 0 & 0 \end{bmatrix}.$$

Here $\mathbf{C}$ is a unit $\mathbf{D}$ is a zero matrices.

The control was realised as shown in *Fig. 4*. On this figure anomaly generated in the rolling moment is shown, too.

The control was realised by feedback control (11). The simple feedback was determined by applicating the optimal linear quadratic problem to the initial system [10]. The other feedback system was designed as the robust feedback controller based on the LQR/LTR algorithm. The feedback matrix was determined application of the software MATLAB.

There are some interesting results of investigation demonstrated on the Figures. The input, e.g. aileron deflection and the modelled anomaly in the rolling moment are shown in the *Fig. 4*. The difference in the systems and their response on the aileron deflection input in case of simple feedback and robust feedback controller can be checked from *Fig. 5*. The effects of additive system anomalies like rolling moment at zero roll angle are shown in *Fig. 6*. The influences of deviation in the state matrix element $\mathbf{A}(2,2)$ are represented by *Fig. 7*.

At last on the *Fig. 8* the interesting effect of additive system anomalies is demonstrated, when the robust feedback controller application has a greater final error than the simple feedback system. In addition to them the final errors in controlled systems have the different signs.

7. Summa

The aim of this paper was to draw the attention to a new theoretical and practical problem caused by operational life-dependent, stochastic changes in the structural and operational characteristics of aircraft systems. These deviations in the characteristics can be called as system anomalies, if they are greater then could be covered in an easy way by modern methods of control and they do not involve the failures or standstills of given systems.

The process of deviations in system characteristics should be controlled in two levels by optimal design of aircraft operational processes including the maintenance and repair and by operative, on-board control systems, including adaptivity and robustness.

For general investigation of given problems we offer to develop the theory of system anomalies. In this paper the elements of the mentioned theory were described and concrete recommendations were offered for possibly available models for description of system anomalies and their effects on the system characteristics.

The developed system anomalies theory was applied to aircraft control systems. In case of automatic control the system anomalies can be taken into account as the deviations in output (motion variables) of systems measured for feedback input. Finally some effects of anomalies on the aircraft control system were demonstrated by the results of investigation of stabilising the aircraft lateral disturbed motion.

References

[1] ROHÁCS, J.: Analysis of Methods for Modelling Real Flight Situations, *17th Congress of ICAS, Stockholm, Sweden, 1990, ICAS Proceedings*, 1990, pp. 2046–2054.

[2] ROHÁCS, J.: Evaluation and Prediction of Permanent Deformation in Delta Wings, *Periodica Polytechnica Transportation Engineering*, BME, 1986, No. 1. pp. 17- 32.

[3] ROHÁCS, J.: Anomalies in the Aircraft Control Systems, *19th Congress of the International Council of Aeronautical Sciences*, Anaheim, CA USA, Sept. 18 - 23 1994'*ICAS Proceedings*, 1994. pp. 1400–1406.

[4] WEINMANN, A.: Uncertain Models and Robust Control, Springer-Verlag, Wien, New York, 1991.

[5] ROHÁCS, J.: On Adaptive Control of Technical System, *9th IFAC/IFORS Symposium, Identification and System Parameter Estimation*, Budapest, Hungary, 1991, pp. 748–753.

[6] BUGAJSKI, D. J. – ENNS, D. F.: Nonlinear Control Law with Application to High Angle-of-Attack Flight, *J. Guide. Control and Dynamics* 1992, No. 3, pp. 761–767.

[7] MCRUER, D. – ASHKENAS, I. – GRAHAM, D.: Aircraft Dynamics and Automatic Control, Princeon University Press, Princeton, New Jersey, 1973.

[8] MCLEAN, D.: Automatic Flight Control Systems, Prentice Hall, 1990.

PERIODICA POLYTECHNICA SER. TRANSP. ENG. VOL. 24, NO. 1, PP. 19-27 (1996)

AERODYNAMIC PARAMETER ESTIMATION OF THE CG CONTROLLED AIRPLANES

Tamás GAUSZ

Department of Aircraft and Ships
Technical University of Budapest
H-1521 Budapest, Hungary
Phone: 36 1 463 1795
e-mail: gausz @ PRO2gjt.bme.hu

Received: November 30, 1994

Abstract

The aim of this work is investigation of the air forces and their moments acting on the hang gliders. The hang gliders have elastic and flexible structure so the distribution of the air forces is characterised by the shape of the sail surface and the sail surface is either determined by the air force distribution. This research work is built on the theoretical calculations and practical measurings. The results of this investigation can be applied principally to flight mechanical calculations of the hang gliders.

Keywords: hang-glider, elastic deformation, load distribution.

1. Introduction

Well known that the hang-gliders have elastic and flexible structure. The load distribution of the air forces is characterised by shape of the sail surface and sail surface is also determined by the air forces distribution . The aim of this work is investigation of the air forces and their moments as a function of the load factor in steady case.

This research work is built on the theoretical calculations and practical measurings. The vortex panel method for the profiles – completed with the ground phenomena of fluid friction (given in [1] and [5]) and the advanced vortex line theory for the finite wings [2],[5] was applied in the theoretical part.

The measuring was executed on a concrete hang-glider type. During it we measured the hang-force of the pilot and the bending moment of the wing bar (near to the connecting point of the cross tube and the wing bar).

2. The Measurements and its Results

The measuring was executed during the flight on the third generation of hang-gliders. The geometrical characteristics shown in *Table 1* refer to the

Table 1.

y	h	α
0	2.679	α+1.05
1.7	2.333	α+1.92
2.555	1.843	α+2.62
3.41	1.642	α+2.62
4.16	1.469	α+1.74
4.9	1.181	α−0.87
5.39	0	0
[m]	[m]	[deg]

normal flight state. Here the y is a spanwise coordinate, h is the chord length and α is the angle of attack.

The normal flight state means that the resultant air force is equal to the weight (G=940 N) and of course the load factor (n) is equal to one.

Distribution of the angle of attack is a very important function. In the next calculations we will follow its varying. For determination the function we used the method of the least squares. The distribution can be approximated by the next polynom:

$$\alpha = a + b|y| + c|y|^2 + d|y|^3. \tag{1}$$

The resultant air force is equal to weight. From this condition we can determine the values of the polynom coefficients:

$a = 0.155000;$
$b = 0.010025;$
$c = 0.009457;$
$d = -\ 0.00249.$

As it is mentioned above the hang-force of the pilot and the bending moment of the wing bar were registrated. The hang-force was translated in a time by 0.998 seconds and its magnitude was transformated. One part of the results along with the beam moment are shown on *Fig. 1.*

It can be established that the covering is suitable. During total measuring time the correlation between two curves is 70.4%. It has been found that the wing bar's bending moment depends a lot on the hang-force. Naturally the other parameters influence this moment too, but fundamentally it is function of the hang-force.

Averaging some suitable intervals of the measurements we have found only two pairs of values (the mean values of the hang-force and the bending moment characterize the different flight states):

(940 N; 208 Nm)
(1756 N; 270 Nm)

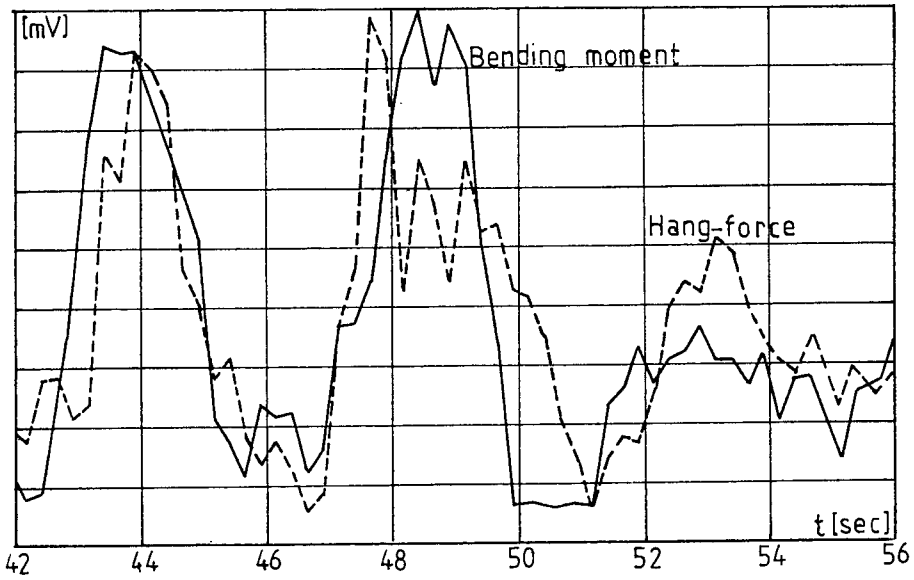

Fig. 1. Bending moment and hang-force

The first one is connected to the normal flight state when the load factor (n) is equal to one. In the second one the load factor is 1.87.

Because of a quite short measuring time it was impossible to choose much more steady considered pairs.

From the previous investigations [3] it can be declare that the maximum hang force is 2317 N with a confidence limit of 99.99%.

Presuming that the bending moment increases as a linear function of the hang force (this assumption gives us higher safety) we will get the maximum bending moment of 310 Nm. So safety coefficient of the braking will be equal to 1.92 .

3. Theoretical Investigations

During the theoretical investigation the first step was parameter identification for the steady flight state (940 N, 208 Nm).

The investigated hang-glider is built from similar profiles, only the chord length and the angle of attack of profiles varies with the wing span, as it is shown in *Table 1.* The profile characteristics are calculated by the advanced vortex panel method [1]. The profile is represented in *Fig. 2.*

The calculated lift-, drag- and moment coefficient - as a function of the angle of attack - are shown in *Table 2.*

It should be noted also that at the angle of attack about 8 degrees

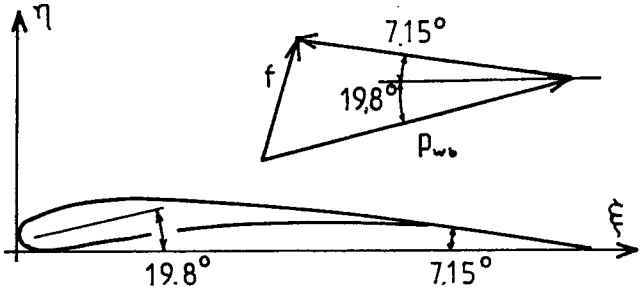

Fig. 2. Wing profile

Table 2.

α	c_L	c_D	c_m
−4	0.05	0.0247	−0.0573
−2	0.279	0.0168	−0.0568
0	0.5	0.0129	−0.0559
2	0.726	0.0058	−0.0546
4	0.95	0.0135	−0.0530
6	1.174	0.0203	−0.0511
8	1.397	0.0315	−0.0488
[deg]	[–]	[–]	[–]

the separation has just begun, thus it gets us the upper limit of the profile calculations.

In the ground load case (n=1) – for the given profile parameters – the lift distribution of spanwise can be calculated by using method [2]. Thus the lift coefficient for each profile of the wing would be found. With knowledge of the lift coefficient the pressure distribution of the chordwise and the resulting force of it can be calculated :

$$\mathbf{f} = \int p \, \mathrm{d}\mathbf{A}; \qquad \text{where} \qquad \mathbf{f} = (f_\xi) f_\eta$$

and p – pressure distribution;
f_ξ – force component in ξ-direction;
f_η – force component in η-direction;
ΔA – wing section surface.

Assuming that the reaction forces at the leading and trailing edge are tangential to the sail (the tangential direction is given in *Fig. 2*) the bending

load distribution along the wing bar can be determined:

$$p_{wb} = [0.3108\ 2.089]\mathbf{f}$$

After double integration the result of the bending moment of the wing bar: 207.4 Nm. The measured bending moment tallies with the calculated one excellently.

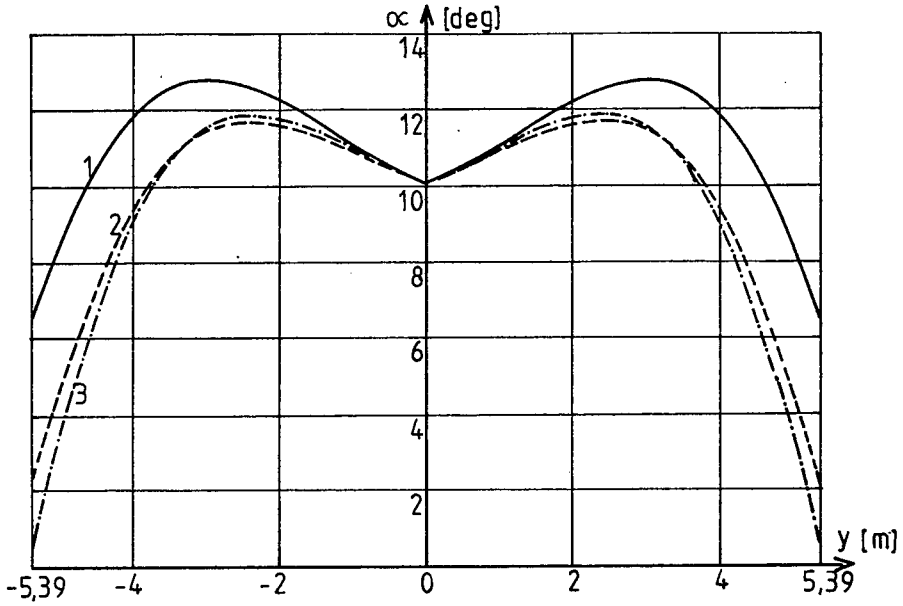

Fig. 3. Angle of attack distribution

The second step of this work is the investigation of the second measured value pair in steady flight state (1756 N, 270 Nm). In calculation a, b, c and d values were variated in such a way that the differences between the resultant air force and the given hang-force as well as the calculated and measured bending moment have to be small enough. The flight speed was chosen in such a way that the a value has to be constant. After calculation we have:

$a =$ 0.155000;
$b =$ 0.010025;
$c =$ 0.006856;
$d =$ −0.00249.

The third extrapolated state (2317 N, 310 Nm, n=2.46) was investigated, too. This is a semi-empirical state. Applying a = const. condition we will get the angle of attack's distribution relatively far from the stall.

Thus the coefficients are:

$a = \quad 0.15500;$
$b = \quad 0.010025;$
$c = \quad 0.008511;$
$d = -0.00299.$

Belonging to these three different cases the distribution of the angle of attack is shown in *Fig. 3.*

In favour of the comparison the a values are equal, thus all of the curves have a common point: it is the angle of attack in the symmetry plane.

If the load factor increases then the distribution curve of the angle of attack along the outer part of the wing relatively decreases. It can be declared, too, that the wing by its own deformation reduces the loading on the outer part of the wing.

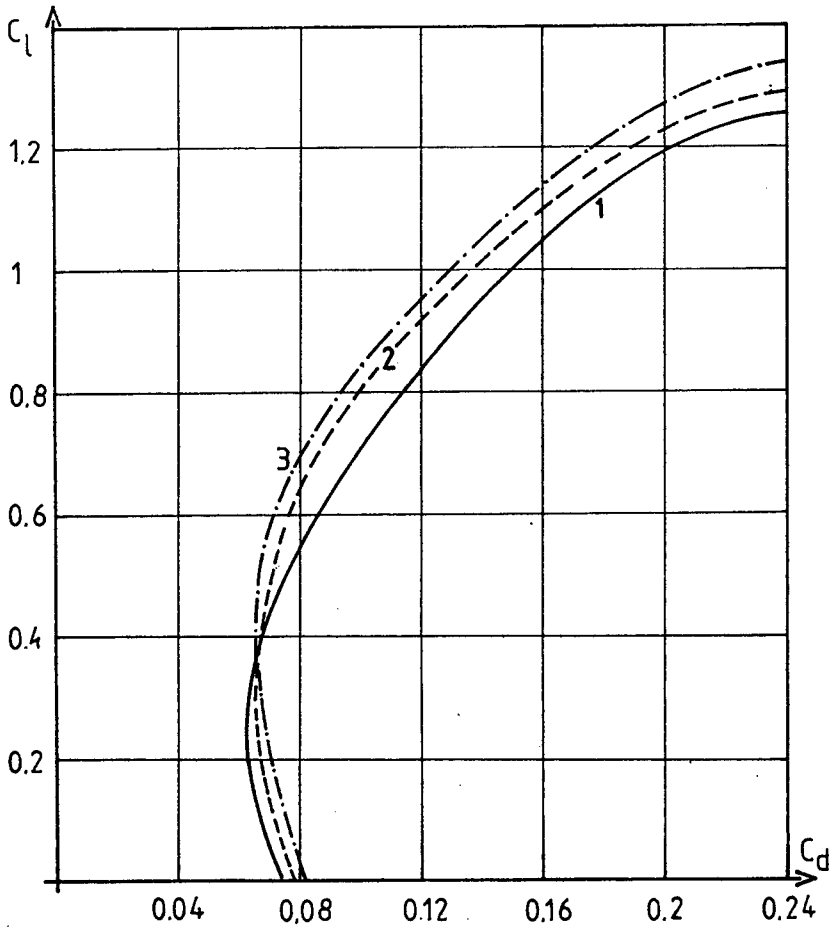

Fig. 4. Polar diagram

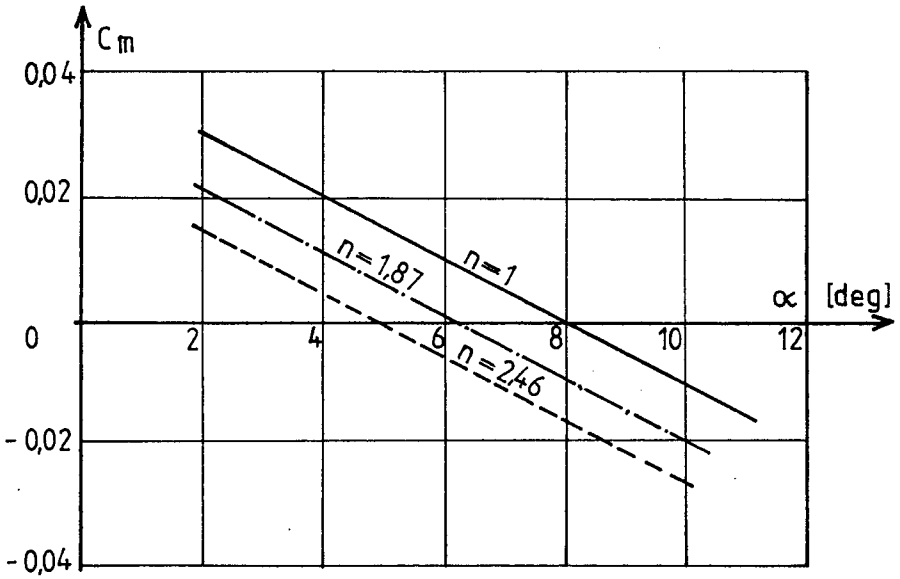

Fig. 5. Calculated moment coefficient

In the investigated interval we can introduce the extension of the angle of attack's distribution:

$$\alpha = a + b|y| + (0.0239 - 0.0208n + 0.063n^2)|y|^2$$
$$+(-0.00388 + 0.00224n - 0.000853n^2)|y|^3$$
$$1 \leq n \leq 2.46 \qquad (2)$$

By this formula we can calculate the distribution of the angle of attack for a given hang-glider type.

4. Aerodynamical Characteristics

On the grounds of these calculations the aerodynamical properties for a given hang-glider can be estimated as a function of the load factor namely the lift coefficient, the drag coefficient and the moment coefficient. In *Fig. 4* we can see the different polar curves. The first curve is given in [4]. (This is an old approximation.) The second curve was calculated on the grounds of the normal flight state and the third is the polar curve with the load factor equal to 1.87. The polar curve for the load factor of 2.46 is practically the same as the third curve.

The slope of the lift coefficient curve is practically constant. The expression of the lift coefficient of the hang-glider as a function of the load

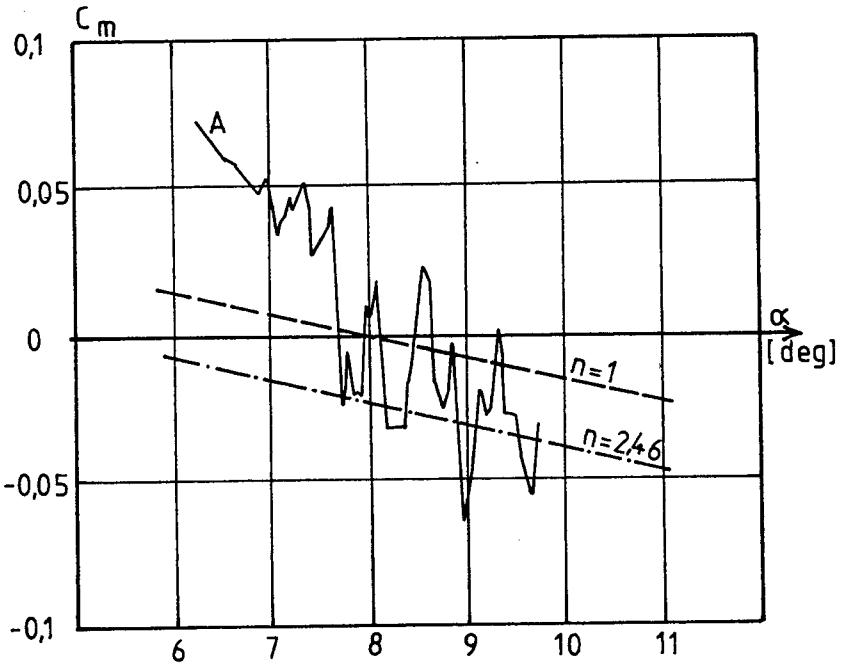

Fig. 6. Identified (A) and calculated moment coefficient

factor and the angle of attack is:

$$c_L = 0.08\alpha + 0.17 - 0.054n \tag{3}$$

$$\text{if} \quad 0 \leq \alpha \leq 0.244$$
$$\text{and} \quad 0 \leq n \leq 2.46$$

The change of the moment coefficient is the most significant and the most interesting thing (see it in *Fig. 5*).

It is very important that the values of the angle of attack at the trim position decrease with the increasing of the load factor. The moment coefficient as a function of the load factor and of the angle of attack (at a given CG position) is:

$$c_m = 0.005\alpha + 0.05052 - 0.01052n \tag{4}$$

$$\text{if} \quad 0 \leq \alpha \leq 0.244$$
$$\text{and} \quad 0 \leq n \leq 2.46$$

This gives us an additional stability. Surely if the hang-glider flies at the angle of attack about 8 degrees and if the disturbance increases the load factor, we would have positive additional moment. This moment decreases the angle of attack, thus the loading would be decreased.

In *Fig. 6* we are comparing the calculated moment coefficients with the identified values of the moment coefficient which can be found in [3]. This curve is marked with 'A'. We can establish a good correlation between these two results. The slope of the mean values of curve 'A' is practically identical with 'n=1' or 'n=2.46' curves. This property characterizes the static stability of the given hang-glider. But a lot of individual points are not between 'n=1' and 'n=2.46' curves, thus the moment coefficient is a function not only of the angle of attack and of the load factor but it depends on other parameters, too – the most important parameter is time derivate of the angle of attack (α).

The results of this calculation can be applied principally to flight mechanical investigation of the hang-gliders.

References

[1] GAUSZ, T.: Investigation and Extension of Validity of Vortex Panel Method Applying to an Airfoil, *Periodica Polytechnica* – in preparation.

[2] GAUSZ, T. Application of Three Dimensional Vortex Theory to the Finite Wings with General Form: *Periodica Polytechnica* – in preparation.

[3] SEREGÉLY, L. – GAUSZ, T.: Siklórepülők repülésmechanikai vizsgálata (Flight Mechanics Investigation of Hang-Gliders – in Hungarian) X. Magyar Repüléstudományi Napok, Szolnok, 1993.

[4] FILKÓ, A.: Siklórepülők repülésmechanikai jellemzőinek vizsgálata (Investigation of Flight Mechanics Characteristics of Hang-Gliders – in Hungarian) Diplomaterv, 1990.

[5] GAUSZ, T.: A felhajtóerő és az indukált ellenállás (Lift and Induced Drag – in Hungarian) BME Areo- és Thermotechnika Tanszék, 1990.

PERIODICA POLYTECHNICA SER. TRANSP. ENG. VOL. 24, NO. 1, PP. 29-46 (1996)

CHANGES IN GAS TURBINE MAPS AS RESULTS OF DIVERGENCE IN GEOMETRICAL PARAMETERS

Imre SÁNTA

Department of Aircraft and Ships
Technical University of Budapest
H-1521 Budapest, Hungary

Received: November 7, 1994

Abstract

The behaviour of the turbines of gas turbine power plants determines decisively the operation of the whole unit. Therefore, the detailed knowledge of it will be required, as well as the determinability of the changes in the operational characteristics as a function of geometrical and other parameters (damage). In this paper, the effect of the change in the geometrical parameters on the turbine characteristics is examined. The method of examination is based on the application of the mathematical model of the turbine. In the paper, the method of the mathematical description of the thermal hydraulic processes at the level of the row of blades, the equations incorporated in the model and the flow-chart of the algorithm for the mathematical model are described. The modification of the characteristics due to the change of the blade angles and the radial clearances is also demonstrated in it.

Keywords: gas turbine modelling, turbine map, losses, efficiency, multistage turbines, row of blades.

Nomenclature

c	–	absolute velocity
w	–	relative velocity, work
u	–	peripheral velocity
T	–	absolute temperature
p	–	absolute pressure
π	–	pressure ratio
n	–	number of revolution
f	–	fuel-to-air ratio
α	–	angle of absolute velocity
β	–	angle of relative velocity
i	–	enthalpy
c_p	–	mass specific heat at constant pressure
κ	–	adiabatic exponent
R	–	specific gas constant
A	–	area
λ	–	non-dimensional velocity

$\pi(\lambda)$ – pressure gas dynamic function
$\tau(\lambda)$ – temperature gas dynamic function
$q(\lambda)$ – non-dimensional mass flow rate
ρ – density
m – mass flow rate
Re – Reynolds number
ξ – loss coefficient
M – Mach number
η – efficiency
P – power
ψ – velocity-loss factor
l – chord of the blade
t – pitch
δ – radial clearance
h – height of the blade

Subscripts

1 – parameter at the inlet of the row of blades
2 – parameter at the exit of the row of blades
j – serial number of the row of blades
T – turbine
cr – critical
w – parameter in relative motion
0 – parameter at the throat
p – profile
t – theoretical (ideal)
u – tangential component
st – stage
fr – friction
te – trailing edge
cl – clearance
m – mean
$cool$ – cooling
mix – mixing
Re – parameter due to Reynolds number
s – isentropic

Superscripts

$*$ – stagnation parameter
$''$ – parameter at the tip diameter
$'$ – parameter at the root diameter

1. Turbine Modelling

Turbine model describes the processes occurring in the rows of blades by aero-thermodynamic equations and determines the exit parameters as function of inlet ones.

The turbine mathematical model is a method of calculation of the turbine map.

1.1. Calculation of the Row of Blade Parameters

The basic equations of calculations were developed from expressions of [1],[2].

Minimum cross-sectional area between blades

$$A_{0,j} = D_{2,j} h_j \pi \sin \beta_{2,j} \,. \tag{1}$$

Parameters of gas at the inlet

Data of velocity triangles

$$w_{1,h} = \sqrt{c_{1,j}^2 + U_{1,j}^2 - 2c_{1,j}u_{1,j}\cos\alpha_{1,j}} \,, \tag{2.a}$$

$$\beta_{1,j} = \tan^{-1} \frac{c_{1,j}\sin\alpha_{1,j}}{c_{1,j}\cos\alpha_{1,j} - u_{1,j}} \,. \tag{2.b}$$

Stagnation enthalpies in absolute and relative motion

$$i_{1,j}^* = c_p T_{1,j}^* \,, \tag{3}$$

$$i_{w1,j}^* = i_{1,j}^* - \frac{w_{1,j}^2 - c_{1,j}^2}{2} \,. \tag{4}$$

Stagnation temperature in relative motion at the inlet

$$T_{w1,j}^* = \frac{i_{w1,j}^*}{c_p} \,. \tag{5}$$

Gas dynamic functions

$$\lambda = \frac{c}{c_{cr}} \,, \quad \tau(\lambda) = \frac{T}{T^*} = 1 - \frac{\kappa - 1}{\kappa + 1}\lambda^2 \,, \quad \pi(\lambda) = \frac{p}{p^*} = \tau(\lambda)^{\frac{\kappa}{\kappa-1}} \,,$$

$$q(\lambda) = \frac{\rho c}{\rho_{cr} c_{cr}} = \lambda \left[\tau(\lambda)\frac{\kappa+1}{2}\right]^{\frac{1}{\kappa-1}} \,. \tag{6}$$

From what

$$\lambda = \left\{ \left[1 - \pi(\lambda)^{\frac{\kappa-1}{\kappa}} \right] \frac{\kappa+1}{\kappa-1} \right\}^{\frac{1}{2}} . \tag{7}$$

Applying these expressions, we can get

$$\pi(\lambda_{1,j}) = \frac{p_{1,j}}{p^*_{1,j}} \quad \text{and} \quad \pi(\lambda_{w1,j}) = \frac{p_{1,j}}{p^*_{w1,j}} . \tag{8}$$

Stagnation pressure in relative motion

$$p^*_{w1,j} = p^*_{1,j} \frac{\pi(\lambda_{1,j})}{\pi(\lambda_{w1,j})} . \tag{9}$$

Mass flow rate of cooling air

$$\dot{m}_{cool,j} = \Delta m_{cool} \dot{m}_{1,j} , \tag{10}$$

where Δm_{cool} is the relative cooling air mass rate at the exit.

Clearance losses [1]

$$\dot{m}_{cl,j} = \dot{m}_{1,j} \frac{\delta D}{h D_m} \left[1 + \frac{0.6}{\sin \beta_{2,j}} \left(\frac{l}{t} \right)^* \right] . \tag{11}$$

Parameters of gas at the exit

Mass flow rate

$$\dot{m}_{2,j} = \dot{m}_{1,j} + \dot{m}_{cool,j} + \dot{m}_{cl,j} . \tag{12}$$

Fuel-to-air ratio

$$f_2 = \frac{f_1}{1 + \left(\frac{\dot{m}_2}{\dot{m}_1} - 1 \right) (1 + f_1)} . \tag{13}$$

Stagnation enthalpy of the gas in relative motion, leaving the row of the blades

$$i^*_{w2,j} = i^*_{w1,j} \frac{\dot{m}_{1,j}}{\dot{m}_{2,j}} + c_p T^*_{cool,j} \frac{\dot{m}_{cool,j}}{\dot{m}_{2,j}} + c_p T^*_{r,j} \frac{\dot{m}_{r,j}}{\dot{m}_{2,j}} + \frac{u_2^2}{2} - \frac{\dot{m}_{1,j}}{\dot{m}_{2,j}} \frac{u_1^2}{2} , \tag{14}$$

where $T^*_{cool,j}, T^*_{cl,j}$ – stagnation temperature of cooling and leakage gases respectively.

From *Eq.* (14) the stagnation temperature of gases in relative motion, leaving the row

$$T^*_{w2,j} = \frac{i^*_{w2,j}}{c_p} . \tag{15}$$

From pressure ratio of the row of blades, the theoretical exit velocity in relative motion:

$$\pi(\lambda_{w2t,j}) = \pi(j) \longrightarrow \lambda_{w2t,j} = \left[\left(1 - \pi(j)^{\frac{\kappa-1}{\kappa}}\right)\frac{\kappa+1}{\kappa-1}\right]^{\frac{1}{2}} . \tag{16}$$

The maximum possible velocity in the slant [1]

$$\lambda_{w2t,\max} = \sqrt{\frac{\kappa+1}{\kappa-1}\left[1 - \frac{2}{\kappa+1}(\sin\beta_2)^{\frac{2(\kappa-1)}{\kappa+1}}\right]} . \tag{17}$$

If $\lambda_{w2t,j} > \lambda_{w2t,\max}$ then $\lambda_{w2t,j} = \lambda_{w2t,\max}$ else the theoretical exit velocity determined by *Eq.* (16).

In the throat if $\lambda_{w2t,j} \geq 1$ then $\lambda_{w0t,j} = 1$ else $\lambda_{w0t,j} = \lambda_{w2t,j}$.

The total enthalpy and the stagnation temperature

$$i^*_{w0} = i^*_{w1,j} + \frac{u^2_{2,j} - u^2_{1,j}}{2} , \quad T^*_{w0} = \frac{i^*_{w0}}{c_p} . \tag{18}$$

The losses of vanes and rotor blades can be divided into two parts:

- losses from the inlet till the throat characterised by velocity-loss factor ψ_{0j}, and
- losses from the throat till the exit (ψ_j).

The following losses are taken into account: profile losses, secondary flow loss and tip clearance loss. Friction losses [1]

$$\xi_{fr} = 0.02185(0.01065x^2 - 2.295x + 160.5)(0.1055y^2 - 0.3427y + 0.295), \tag{19}$$

where

$$x = \begin{cases} \beta_1 + \beta_2 & \text{if} \quad \beta_1 + \beta_2 < 110^0 \\ 110^0 & \text{if} \quad \beta_1 + \beta_2 \geq 110^0 \end{cases} \qquad y = \begin{cases} \frac{\sin\beta_1}{\sin\beta_2} & \text{if} \quad \frac{\sin\beta_1}{\sin\beta_2} < 1.7 \\ 1.7 & \text{else} \end{cases} .$$

Trailing edge losses and losses due to Reynolds number [1]

$$\xi_{te} = 0.2\frac{\delta_k}{t\sin\beta_2} , \quad \Delta\xi_{Re} = \frac{2100}{Re} - 0.021 , \tag{20}$$

where $Re = \frac{\rho_2 w_2 l}{\mu}$, $\mu = (0.229x^3 - 1.333x^2 + 4.849x + \frac{0.275}{\alpha})10^{-5}$,

$$x = \frac{T}{10000} , \quad \alpha \text{ is the air excess factor.}$$

Profile losses

$$\xi_p = \xi_{fr} + \xi_{te} + \Delta\xi_{Re} . \tag{21}$$

Increase in profile losses due to impact and secondary flow losses [1]

$$\Delta\xi_i = a(1-\xi_p)\left(\frac{\beta_{1g}-\beta_1}{\beta_1}\right)^2, \quad \xi_s = 2\xi_p\frac{t\sin\beta_2}{h_2}. \tag{22}$$

Losses of mixing [1]

$$\xi_m = \frac{\dot{m}_{cool,j}}{\dot{m}_{1,j}}\left(1-\frac{c'_{1,j}}{c_{2,j}}\right)^2, \tag{23}$$

where $c'_{1,j} = \frac{\dot{m}_{cool}}{\rho A_{cl,j}}$ and $A_{cl,j} = \frac{h_{cl,j}\delta_{cl,j}D_{m1,j}}{t_j}$. Velocity coefficient in the throat

$$\psi_{0,j} = \sqrt{1-(\xi_{fr}+\xi_s+\Delta\xi_{Re}+\Delta\xi_i)}, \tag{24}$$

and at the exit

$$\psi_j = \sqrt{1-(\xi_{fr}+\xi_s+\xi_k+\Delta\xi_{Re}+\Delta\xi_i+\xi_e)}. \tag{25}$$

The non-dimensional velocities

$$\lambda_{w0,j} = \lambda_{w0t,j}\psi_{0,j}, \quad \lambda_{w2,j} = \lambda_{w2t,j}\psi_j. \tag{26}$$

The pressure ratio can be determined by gas dynamic functions

$$\frac{p_{2,j}}{p^*_{w1,j}} = \pi(\lambda_{w2t,j}), \quad \frac{p_{2,j}}{p^*_{w2,j}} = \pi(\lambda_{w2,j}), \quad \frac{p_{0,j}}{p^*_{w0,j}} = \pi(\lambda_{w0t,j}), \quad \frac{p_{0,j}}{p^*_{w0,j}} = \pi(\lambda_{w0,j}).$$

Stagnation pressure in relative motion after the row of the blades and in throat

$$p^*_{w2,j} = p^*_{w1,j}\frac{\pi(\lambda_{w2t,j})}{\pi(\lambda_{w2,j})}, \quad p^*_{w0,j} = p^*_{w1,j}\frac{\pi(\lambda_{w0t,j})}{\pi(\lambda_{w0,j})}. \tag{27}$$

The mass flow rate of the row of blades

$$\dot{m}_{0,j} = \frac{p^*_{w0,j}A_{0,j}q(\lambda_{w0,j})}{\sqrt{T^*_{0,j}}}\sqrt{\frac{\kappa}{R}\left(\frac{2}{\kappa+1}\right)^{\frac{\kappa+1}{\kappa-1}}}. \tag{28}$$

Mass flow rate entering the row of blades

$$\dot{m}_{1,j} = \dot{m}_{,j}. \tag{29}$$

The exit mass flow rate

$$\dot{m}_{2,j} = \dot{m}_{1,j} + \dot{m}_{cool,j} - \dot{m}_{l,j}. \tag{30}$$

The relative exit velocity

$$w_{2,j} = \lambda_{w2,j}c_{cr}. \tag{31}$$

The exit Mach number

$$M_{2,j} = \lambda_{2,j}\sqrt{\frac{2}{(\kappa+1)\tau(\lambda_{2,j})}}\,. \tag{32}$$

Calculation of the flow deviation in the slant.

The exit angle [3]

$$\beta_{2,j} = \begin{cases} B_1 & \text{if} \quad M_{2,j} \le 0.5, \\ B_2 & \text{if} \quad 0.5 < M_{2,j} \le 1, \\ B_2 + \sin^{-1}\left(\frac{\sin\beta_{2g,j}}{q(\lambda_{w2,j})}\right) - \beta_{2g,j}. \end{cases} \tag{33}$$

where

$$\begin{aligned} B_1 &= \left(1.1325\beta_{2g,j} - 1.925 + 4\frac{t}{e}\right)\frac{\pi}{180}\,, \\ B_2 &= \left[1 + 0.185\left(\frac{t}{e}\right)^2 + 0.03994\frac{t}{e}\right]\beta_{2g,j}^{rad}\,. \end{aligned}$$

The discharge absolute velocity from velocity diagram and the angle

$$c_{2,j} = \sqrt{w_{2,j}^2 + u_{2,j}^2 - 2c_{2,j}u_{2,j}\cos\beta_{1,j}}\,, \quad \alpha_{2,j} = \tan^{-1}\frac{w_{2,j}\sin\beta_{2,j}}{w_{2,j}\cos\beta_{2,j} - u_{2,j}}. \tag{34}$$

Stagnation enthalpy of the gas at the exit before mixing in the cooling air

$$i_{2,j}^* = i_{w2,j}^* - \frac{c_{2,j}^2 - w_{2,j}^2}{2}\,. \tag{35}$$

Non-dimensional discharge absolute velocity

$$\lambda_{2,j} = \frac{c_{2,j}}{c_{cr}}\,. \tag{36}$$

Static and stagnation pressure in absolute motion

$$p_{2,j} = p_{w1,j}^*\pi(\lambda_{w2t,j})\,, \quad p_{2,j}^* = p_{2,j}\pi(\lambda_{2,j})\,. \tag{37}$$

Static discharge temperature

$$T_{2,j} = T_{2,j}^*\tau(\lambda_{2,j})\,. \tag{38}$$

The absolute exit parameters of the row of blades will be the inlet parameters for the next row.

The set of non-linear equations will be composed from mass conservation equations for the rows of the blades.

$$\dot{m}_{1,j} + \dot{m}_{cool,j} + \dot{m}_{r,j} - \dot{m}_{2,j} = 0\,, \quad j = 1,\ldots,n\,. \tag{39}$$

The set of equations can be solved by numerical method.

1.2. Parameters of the Stages

After the calculation of a stator and a rotor row of the blades, it is necessary to find the parameters of the stage.

The actual power is determined as the power of the gas decreased by losses due to tip leakage and amount of heat rejected by cooling air

$$P_f = \dot{m}_{1,j-1}(i^*_{1,j-1} - i^*_{2,j})(1 - \Delta\eta_{leak}) - \dot{m}_{cool,j} c_p \Delta T_{cool,j} \,. \tag{40}$$

where decrease in efficiency due to leakage losses [1]

$$\Delta\eta_{leak} = \frac{\delta D'' \rho''}{h D_m \rho_m} \left[1 + \frac{0.3}{\sin\beta_{2g}} \left(\frac{l}{t}\right)''\right] , \tag{41}$$

change in temperature of cooling air

$$\Delta T_{cool,j} = T''_{cool,j} - T'_{cool,j} \,. \tag{42}$$

Pressure ratio for the stage and exit stagnation temperature

$$\pi^*_{st} = \frac{p^*_{2j}}{p^*_{1,j-1}} , \quad T^*_{2s,j} = T^*_{1,j-1} \pi^{*\frac{\kappa-1}{\kappa}}_{st} \,. \tag{43}$$

Isentropic power for the stage

$$P_{s,st} = \dot{m}_{1,j} c_p (T^*_{1,j-1} - T^*_{2s,j}) \,. \tag{44}$$

Isentropic efficiency

$$\eta^{st}_s = \frac{P_{st}}{P_{s,st}} \,. \tag{45}$$

The exit stagnation enthalpy from energy balance

$$i^*_{2,j} = \frac{\dot{m}_{1,j-1}\left[i^*_{2,j} - (i^*_{1,j-1} - i^*_{2,j})\frac{\dot{m}_{leak}}{\dot{m}_{1,j-1}}\right] + \dot{m}_{cool,j} c_p T''_{cool,j}}{\dot{m}_{2,j}} \,. \tag{46}$$

1.3. Turbine Parameters

Stagnation temperature, non-dimensional velocity and stagnation pressure at the exit

$$T^*_2 = \frac{i^*_{2,j}}{c_p} , \quad \lambda_2 = \lambda_{2,j}\sqrt{\frac{T^*_{2,j}}{T^*_2}} , \quad \dot{p}_2 = \frac{p_{2,j}}{\pi(\lambda_2)} \,. \tag{47}$$

Non-dimensional mass flow rate for the turbine

$$q(\lambda)_T = q(\lambda)_1 \,. \tag{48}$$

Actual power of the turbine

$$P_T = \sum_{i=1}^{z/2} P_{st_i} \,. \tag{49}$$

Stagnation pressure ratio for the turbine

$$\dot{\pi}_T^* = \prod_{i=1}^{z/2} \pi_{st_i}^* \,. \tag{50}$$

Isentropic power of the turbine

$$P_{T_s} = \dot{m}_{1,2} c_p T_{1,1}^* \left[1 - (\pi_T^*)^{\frac{1-\kappa}{\kappa}}\right] \,. \tag{51}$$

Isentropic efficiency

$$\eta_{s_T} = \frac{P_T}{P_{T_s}} \,. \tag{52}$$

1.4. Calculation of $\lambda_u = const.$ Curves on Turbine Characteristics

The calculation concerning the given non-dimensional peripheral velocity

$$\lambda_u = \frac{u}{\sqrt{\frac{2\kappa}{\kappa+1} R T_{1,j}^*}} \tag{53}$$

can be continued by the variation of the pressure ratio of the first row of blades (by the reduction of the pressure ratio from $\pi(j) = 0.9$). In the course of calculations, one of the rows of blades will reach the critical operational mode (choking), and therefore its mass flow rate increase will stop and reaches its maximum value with the given λ_u, and further on the pressure distribution and the flow conditions will not change with the rows of blades preceding the latter one.

Subsequently, the variation of pressure ratio should be continued with the row of blades having reached the critical operational mode, and the equations associated with the former rows of blades should be separated from the system of equations for the mass flow rate conservation. Accordingly, the number of the independent variables $[\pi(j)]$ will also be reduced. The reduction of the pressure ratio should be continued up to the point when the critical operational mode occurs with another row of blades. In this case and afterwards, too, this procedure should be performed according to those described above until the choking occurs with the last row of blades, and the lower limit of pressure ratio range of the turbine to be calculated is reached. In the computing program, the search of the pressure ratio belonging to

the critical operational mode is ensured by automatic step-halving of the pressure ratio in the neighbourhood of the critical operational mode. Then, after the separation of the choked part, the calculation can be resumed anew with the original step interval.

The simplified flow diagram of the calculations is shown on *Fig. 1.*

The temperature and constituent dependence of the specific heat and the adiabatic exponent, as well as the constituent dependence of the gas constant are taken into consideration with the help of the subroutine developed for this purpose.

The significance of the method elaborated for the computation of characteristics lies in the fact that it renders possible the direct determination of the characteristics of multi-stage turbines. There is no need for stage by stage calculation and then for the summation of characteristics – though a possibility is provided of displaying the data by stages, too. The Newton–Raphson method applied to the solution of the set of non-linear equations ensured a very rapid convergence.

Eqs. (39) and the relationships covered by those constitute the mathematical model of the turbine, which can be adapted directly on the models of the other units of gas turbine power plants.

2. Results of Turbine Characteristics' Calculations

Fig. 2 shows the maps of a single-stage and a double-stage gas turbine. On the vertical axis of the turbine characteristics built up of non-dimensional parameters, the non-dimensional mass flow rate developed in the minimum cross-section of the stator blades of the first stage and the turbine efficiency was represented, while the pressure ratio of the turbine was plotted on the horizontal axis. The non-dimensional peripheral velocity λ_u was a parameter. The constant sections $q(\lambda)$ seen on the characteristics show the fact that with the given pressure ratio, a choking occurred in a row of blades of the turbine.

In case the choking occurred for the first time in the row of stator blades of the first stage, then $q(\lambda) = 1$, while the straight sections $1 > q(\lambda) =$ constant seen on the double-stage characteristics (*Fig. 2b*) show that with a given value λ_u, a choking will occur first not in the nozzle of the first stage. As it is shown in the *Fig. 3* and *4* representing the variation of the mass flow rate and the pressure ratio as taking place in the rows of blades, this choking will occur in the third row of blades of the turbine examined. The diagrams on right side show the characteristics in case of decrease of the first stage nozzle exit angle.

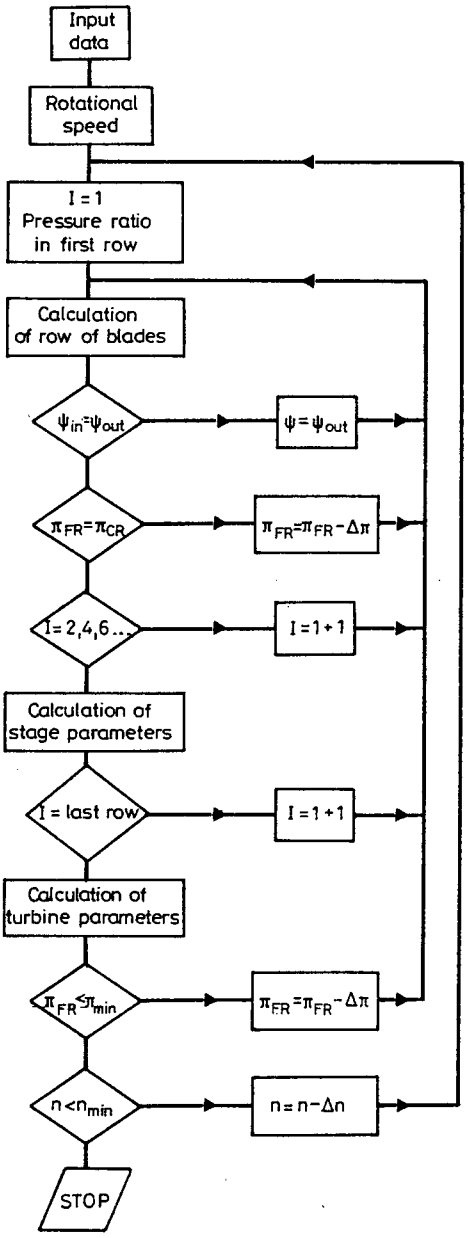

Fig. 1. Simplified flow diagram of the turbine model

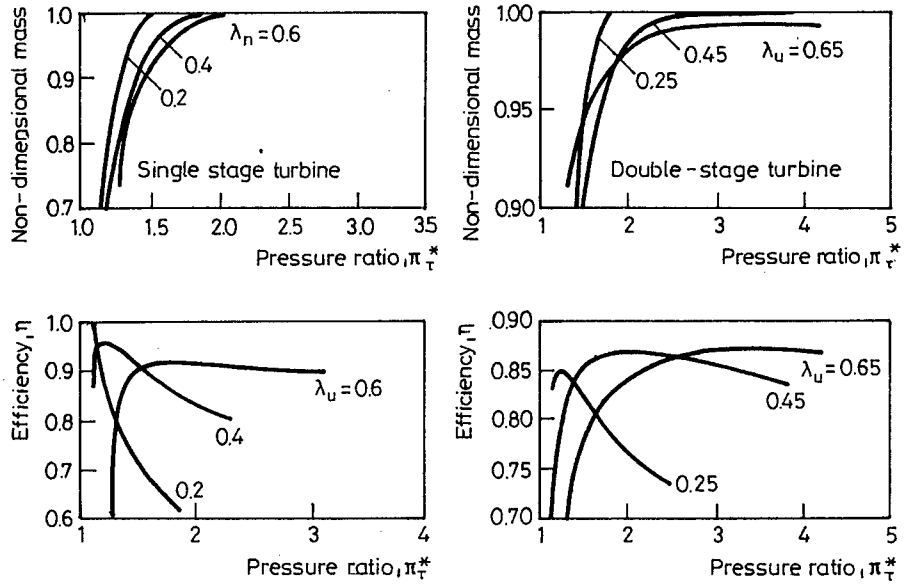

Fig. 2. Calculated turbine maps

3. Effect of Changes in Geometrical Parameters on Turbine Maps

The detailed turbine examinations were performed with the help of the turbine model for the two-stage gas generator turbine unit. In the course of examination, the inlet and outlet angles of blading by each row of blades, as well as the value of radial clearances of rotor blades were varied. The results of calculations are represented on *Figs. 5* and *6*. The dashed lines show a map of the turbine changed geometry.

The analysis of the calculation results as broken down to the level of the row of blades shows that the simulated variations will modify the turbine characteristics (*Figs. 5* and *6*). Depending on the character and measure of variations, the following characteristics will also be changed: the pressure ratio of the turbine as associated with the choking, the sequence of the choking the rows of blades, and as a consequence, the passing capacity of the turbine, as well as its efficiency.

Since the determination of the turbine characteristic of the models examined will take place on the basis of the geometrical characteristics of the turbine in question, this kind of examination will show the way to the correction of calculated characteristics.

From the detailed analysis of the results it can be established that the reduction in the outlet angle of the first-stage row of stator blades –

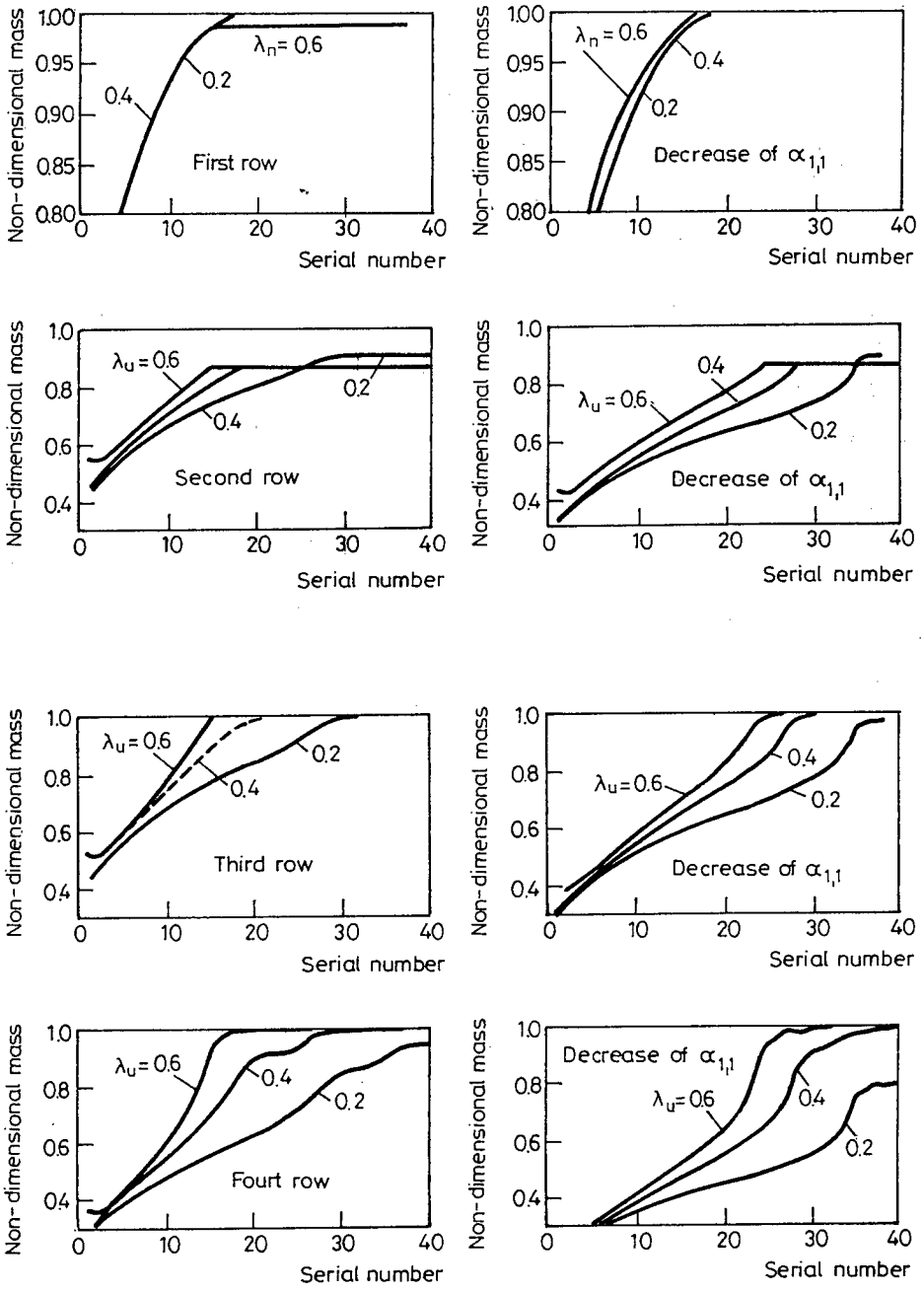

Fig. 3. Mass flow rate variations in the rows of blades

which, in turn, involves also the reduction in the cross-section – will shift the $\lambda_u = \text{const.}$ curves towards the lower pressure ratios of the turbine (*Fig. 5*). This result emanates from the fact that the reduction in cross-section will bring forward the chocking with the row of blade, i.e. the value of $q(\lambda)$ will increase. In this case the reduction of the outlet angle is performed with another row of blade subsequent to the first one, the mass flow rate curves will be shifted towards the higher pressure ratio of the turbine. These reductions in the cross-section will reduce the non-dimensional mass flow rate of the first row of blades, and this, in turn, will be reflected in the diagram.

The increase of radial clearances (*Fig. 6*) will bring no change in the path of the mass flow rate curves with the first or the second stages. The curves of efficiency will be shifted, in both cases, towards the reduction of them.

The highest non-dimensional mass flow rate will be obtained in case the choking occurs with the first-stage row of stator blades. In the case of an increase in the rpm, or more exactly in λ_u, the degree of reaction of the stage(s) will increase, and due to it, the non-dimensional mass flow rate of the stator blades row of the first stage will decrease, and the chocking can occur somewhere downstream, or, even with the row of rotor blades, respectively. (This process will last while β_1 is less than 90°, afterwards a reduction in the degree of reaction will occur.). The constant curves λ_u will be shifted towards the higher pressure ratios and downwards.

From the diagram a similar conclusion can be inferred concerning T_3^* – but due to the fact that it occurs in the denominator of λ_u with the opposite effect – the increase of the temperature will involve the decrease of the degree of reaction, and the non-dimensional mass flow rate will increase.

According to the examinations performed so far, the change in the inlet angle of the rotor blades will not modify considerably the non-dimensional mass flow rate. The reduction of the inlet angle will result in the widening to a small extent of the mass flow rate diagram, while its increase will narrow it. The values of efficiency will be modified due to the change in the angle of attack.

As a result of this examination, a possibility will be provided of designing an optimal turbine construction, as well as the correct determination of the character of turbine damage – in case of spacing out proper measuring points – when the turbine model of this level is integrated into the whole of the power-plant model.

4. Summary

The applied model is suitable – with the knowledge of the geometrical dimensions and the thermodynamic parameters – for the calculation of char-

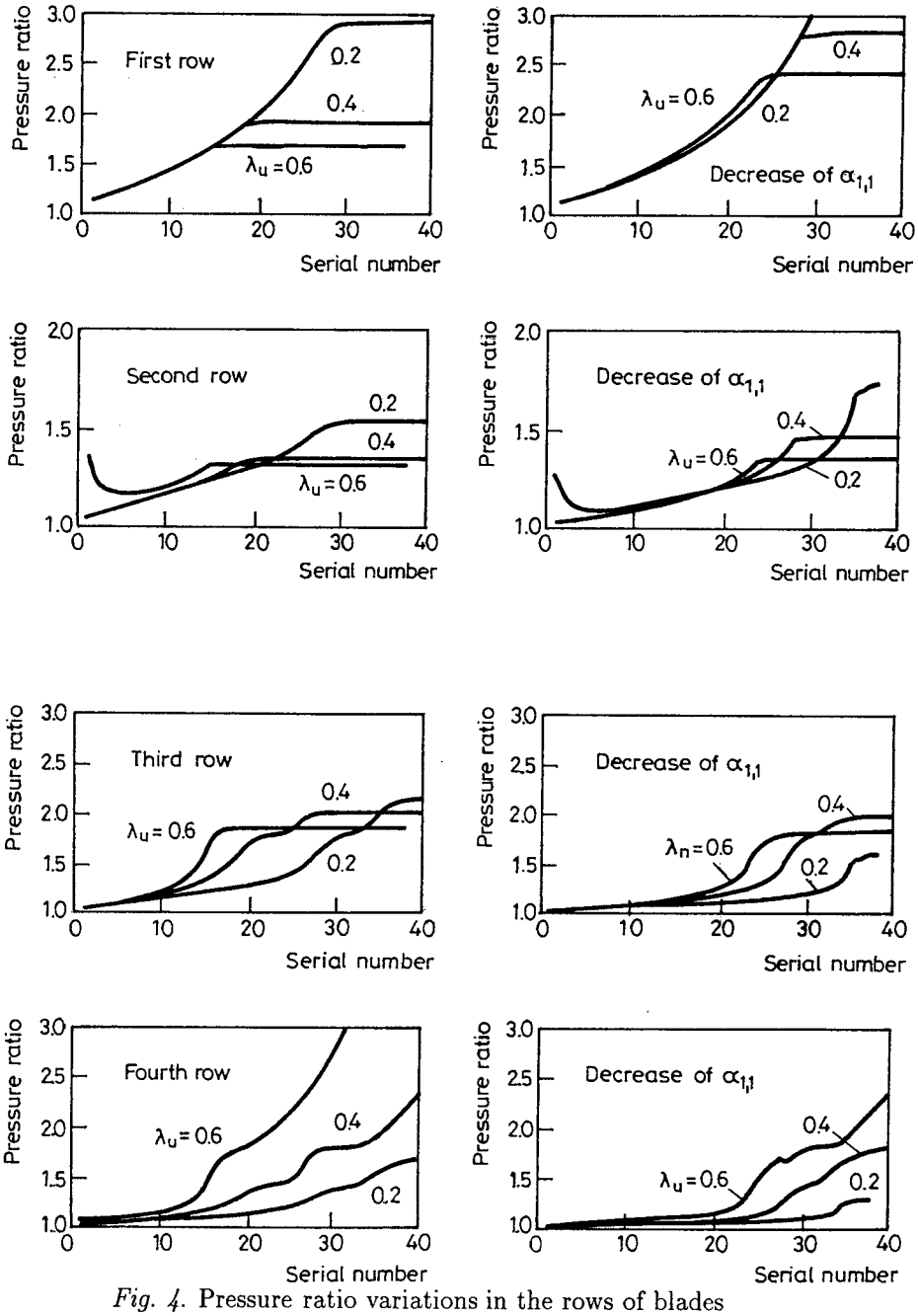

Fig. 4. Pressure ratio variations in the rows of blades

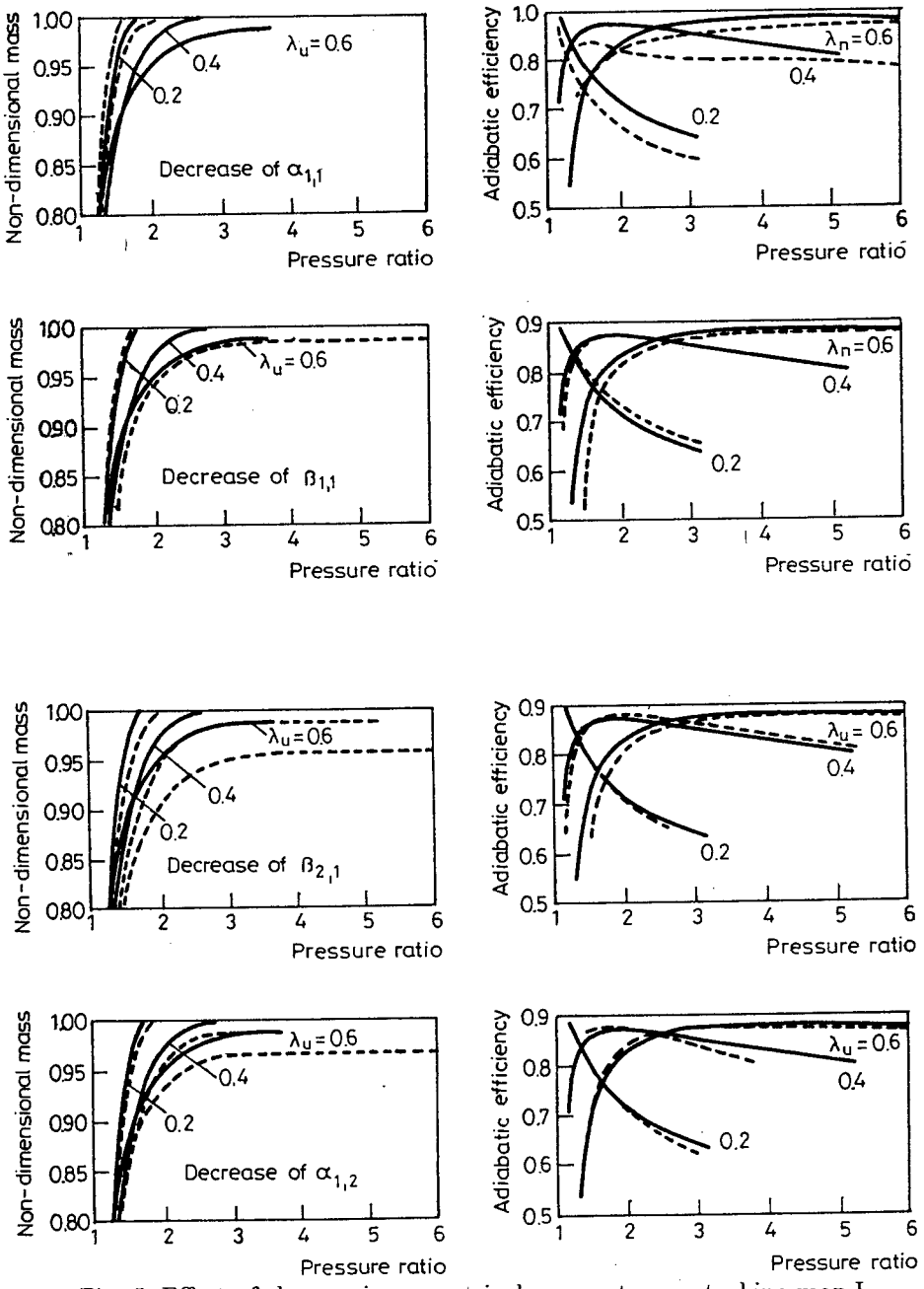

Fig. 5. Effect of changes in geometrical parameters on turbine map I

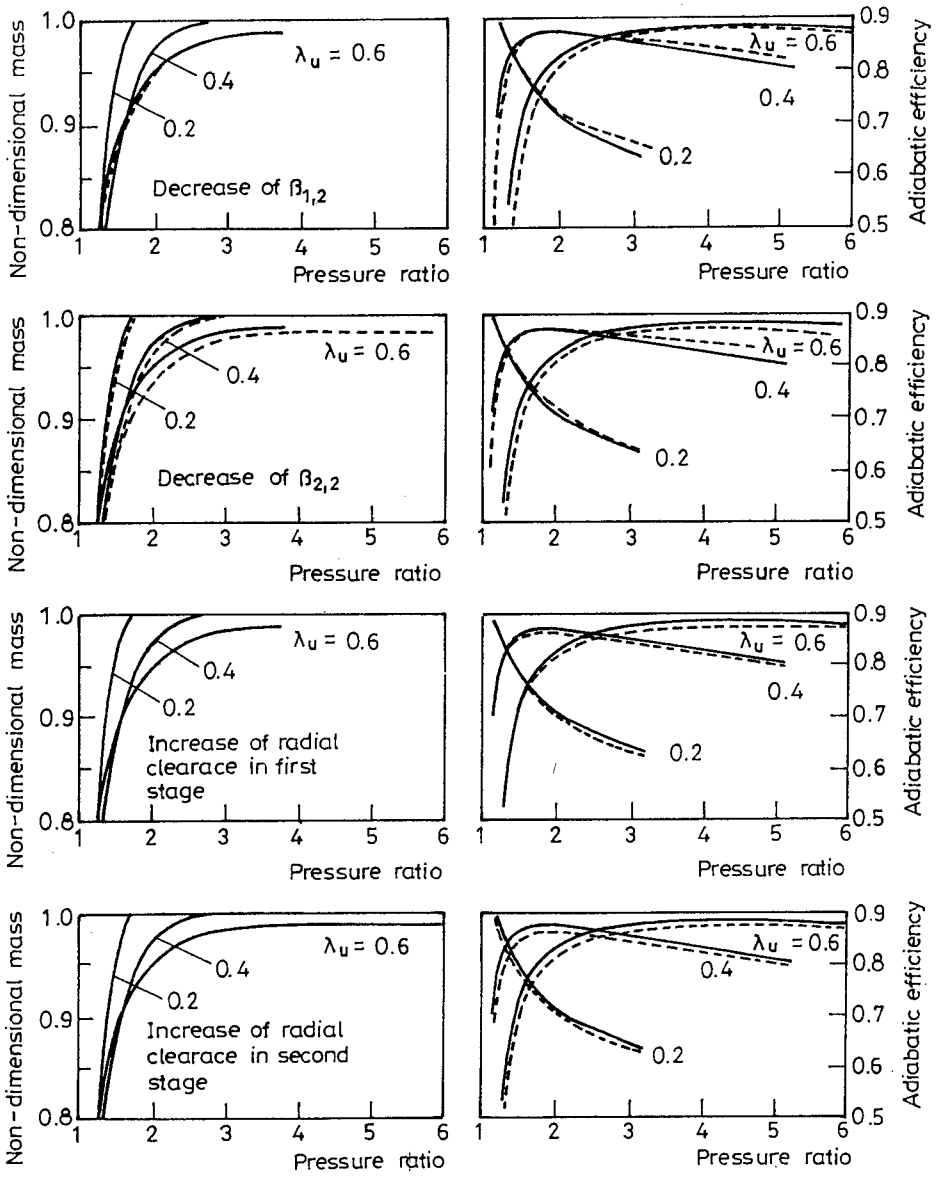

Fig. 6. Effect of change in geometrical parameters on turbine map II

acteristics and the examination of the processes taking place within the turbine in the course of both the design and operation. This model can be inserted – as a component model – into the mathematical model of the gas turbine power plants [4].

The examinations performed already, or to be performed later on, respectively, will provide information about the tendencies and possibilities of model adaptation.

The analysis of the calculation results as broken down to the level of the row of blades shows that the simulated variations will modify the turbine characteristics. Depending on the character and measure of variations, the following characteristics will also be changed: the pressure ratio of the turbine as associated with the choking, the sequence of the choking the rows of blades, and as a consequence, the passing capacity of the turbine, as well as its efficiency.

Acknowledgements

The author would like to acknowledge the support of Hungarian Oil Gas Indrusty Co., Hungarian Airlines MALEV and the Hungarian Scientific and Research Fund.

References

[1] ABIANC, B. H.: Teorija aviacionnüh gazovüh turbin, Masinosztroenie, Moscow, 1979.
[2] COHEN, H. – ROGERS, G. F. C. – SARAVANAMUTTOO, H. I. H.: Gas Turbine Theory, Longman, 1989.
[3] MUKHERJEE, D. K.: Berechnung der Druckziffer einer Turbine, *Z. Flugwiss.*, Vol. 16. 1968.
[4] SÁNTA, I.: Non-linear Mathematical Thermal Models of Gas Turbine Engines and Their Application in Operation, *ICAS Proceedings 1990*, Stockholm, Sweden, pp. 2264–2270.

PERIODICA POLYTECHNICA SER. TRANSP. ENG. VOL. 24, NO. 1, PP. 47-64 (1996)

FROM NON-HOLONOMIC CONSTRAINT EQUATION TO EXACT TRANSPORT ALGORITHM FOR ROLLING CONTACT

Friedrich BÖHM

Department of Mechanics
Technical University of Berlin
D–10587 Berlin, Germany

Received: November 2, 1994

Abstract

The one-point contact problem roughly describing the rolling behaviour of wheels and the sliding behaviour of sleds was defined by Hertz, Cartheodory, Hamel and others. Extending this idea to a continuous field of contact points in a closed 2-dimensional domain produces the nonstationary field of tractrices in the contact area. One has to solve nonlinear partial first order differential equations or integral equations. Discretisation of the whole wheel in dynamic contact gives rise to a new method which is not based on finite element method. Measurements and computations of rolling wheels on a glass plate show that high frequency behaviour of the contact of wheels has to be taken into account to understand all phenomenas.

Keywords: non-holonomic constraints, transport equations, friction, stability, rough contact.

1. Introduction

The one-point contact problem roughly describing the rolling behaviour of wheels and the sliding behaviour of sleds was first solved by Hertz, later on by Caratheodory, Hamel, Neimark and Fuvaev and others. The analytical expression for a pure rolling condition is shown in *Fig. 1* and because of the fact that the angle α for rolling must be zero there exists a differential condition $\mathbf{e}_n \cdot d\mathbf{s} = 0$ or

$$-\sin\psi dx_1 + \cos\psi dy_1 + 0d\psi + 0dt = 0$$

and a rolling condition:

$$dx_1 \cos\psi + dy_1 \sin\psi = Rd\varphi,$$

with the components to be seen from *Fig. 1.*

$$\frac{dx_1}{dt} = \dot{x}_1 = v_{\text{Roll}} \cos\psi, \quad \frac{dy_1}{dt} = \dot{y}_1 = v_{\text{Roll}} \sin\psi,$$

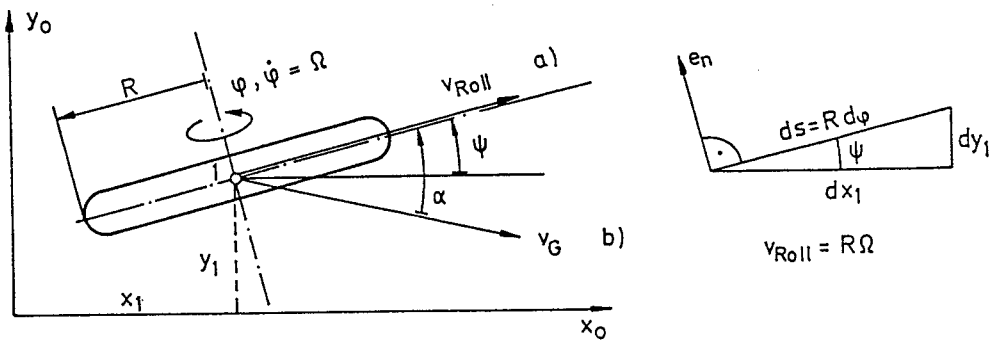

Fig. 1. Rolling wheel: fixed plane x_0, y_0, contact point x_1, y_1, sliding velocity v_G, rolling velocity v_{Roll}, radius of wheel R, angular velocity Ω, increments of moving $dx_1, dy_1, \mathbf{e}_n$, unit vector of wheel axle, direction of wheel plane ψ, non-holonomic condition is $\alpha = 0$ and $v_G = v_{\text{Roll}}$

which is a 'Pfaff's' form. The heading angle ψ is a free parameter and must not be chosen continuously in time. The two differentials dx_1 and dy_1 cannot be integrated because of the fact that the factors $-\sin\psi$ and $\cos\psi$ should hold the

$$\boxed{\text{condition}} \text{ of integrability:}$$

$$df = \frac{\partial f}{\partial x_1}dx_1 + \frac{\partial f}{\partial y_1}dy_1 + \frac{\partial f}{\partial \psi}d\psi + \frac{\partial f}{\partial t}dt \ldots \quad \text{if} \quad \boxed{\frac{\partial^2 f}{\partial x_i \partial x_j} = \frac{\partial^2 f}{\partial x_j \partial x_i}}$$

which obviously they do not (therefore it is called non-holonomic constrained condition). In analytical mechanics it was shown by Appel, Pfaff and Routh that such a condition can be used together with the equations of Newton. In the case of a skater-shoe which belongs to the same condition we get, see in *Fig. 2*, the following acceleration vector for the center of gravity:

$$\begin{aligned} a_x &= \dot{v}_x - \omega v_y - \omega^2 a, \\ a_y &= \dot{v}_y - \omega v_x - \dot{\omega} a\,. \end{aligned}$$

After some manipulations, see Appendix 1, we find the following condition for the heading angle $\psi : \dot{\psi} = \omega$,

$$\dot{\omega} + \lambda\omega = 0\,, \quad \lambda = \frac{mav_x}{J_s + ma^2}\,.$$

For the starting conditions that the velocity v_x and $\dot{\psi}$ are also constant, the parameter a shows that there are two solutions possible. One solution is stable the other one unstable. If the center of gravity is in front of the

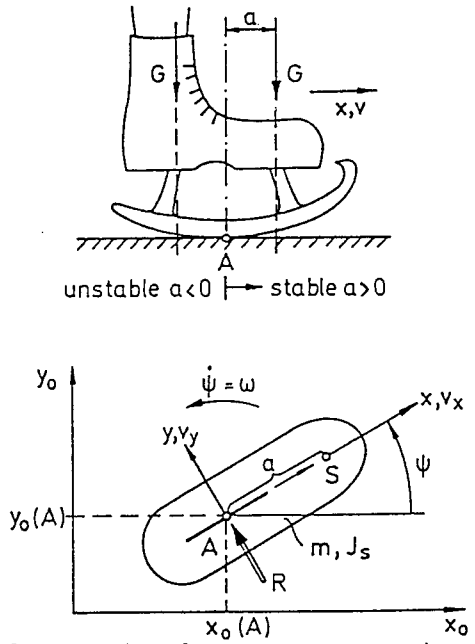

Fig. 2. Ice-skating shoe: moving plane x, y, contact point A, weight of skater G, distance to C.G (=S) is a non-holonomic condition $v_y = 0$.

contact point the solution is stable. Otherwise the solution is unstable. In this case the motion of the system produces also singular points where the center of gravity is rotating around the contact point which is fixed a moment in the contact plane. From this behaviour one can conclude that every vehicle equipped with laterally not stiff front wheels and stiff rear wheels is stable (understeering).

In reality wheels show a small amount of deformation when rolling forces laterally or longitudinally occur. In *Fig. 3* the lateral force is produced by a constant deformation $\overline{y}$ and linear increasing deformation of the profile elements along the contact length of a deformable wheel. B. v. SCHLIPPE and R. DIETRICH and also RIEKERT have shown that at the front of the contact area a non-holonomic rolling condition can be defined with a heading angle ψ relative to the plane of the wheel. Using the assumption that the deformation laterally of the leading point of contact is proportional to the created lateral force and it is also proportional to the heading angle ψ we get the so-called 'relaxation length' L which marks a point on the x axis around which a simulated swiveling 'leading wheel' is rotating. Using the non-holonomic constraint equation for this leading wheel one can derive the differential equation of first order in time for the linear behaviour of the lateral force generation of the wheel (see Appendix 2). Today this differential

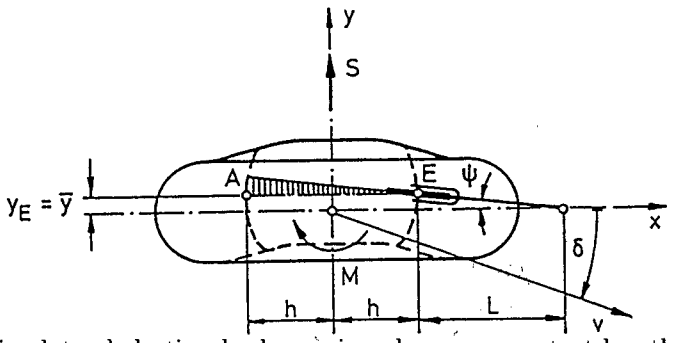

Fig. 3. Rolling lateral elastic wheel: moving plane x, y, contact length $2h$, cornering force S, cornering moment M, concerning angle δ, swiveling angle ψ, lateral global deformation $\overline{y}$, entrance E, outlet A, local deformation at A is $2h\psi$, relocation length is L, simple model, load slowly changing.

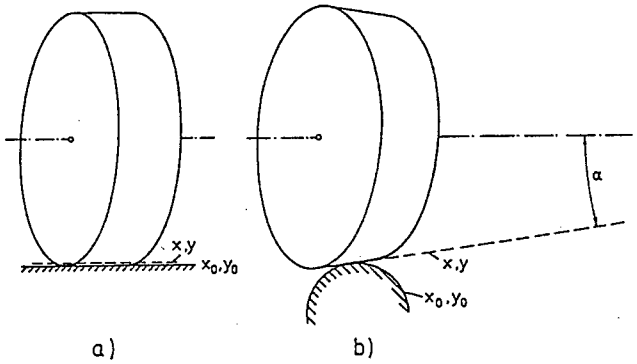

Fig. 4. Two surfaces which can be flattened without deformation: a small penetration of two elastic bodies produces small tangential deformation and can be added to the relative motion of the two planes, cone angle produces spin.

equation is generally used in industry. It can be used also for longitudinal forces by aid of a shorter relaxation length.

There are three statements which need to improve this equation:

1. The area of contact has a deformation field perhaps with short wavelength which is only poor approximated by linear increasing deformation with contact length.
2. The real pressure distribution does not allow tangential forces bigger than the friction limit.
3. Non-smooth surfaces need a discontinuous theory.

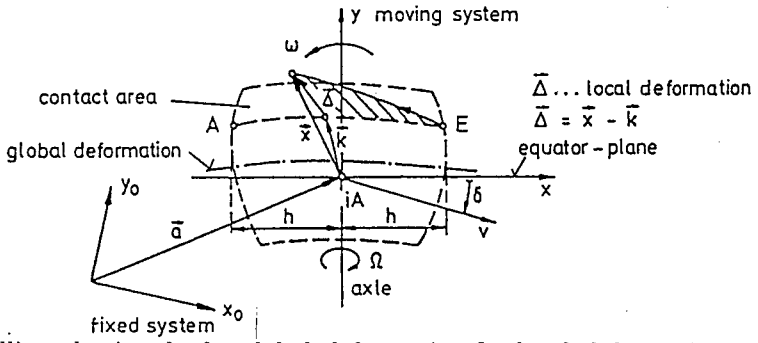

Fig. 5. Rolling elastic wheel: global deformation $\mathbf{k}$, local deformation $\mathbf{\Delta}$, fast changing contact area $h = h(t)$, fast changing of $\delta(t)$, $v(t)$, $\omega(t)$ and load, complex model

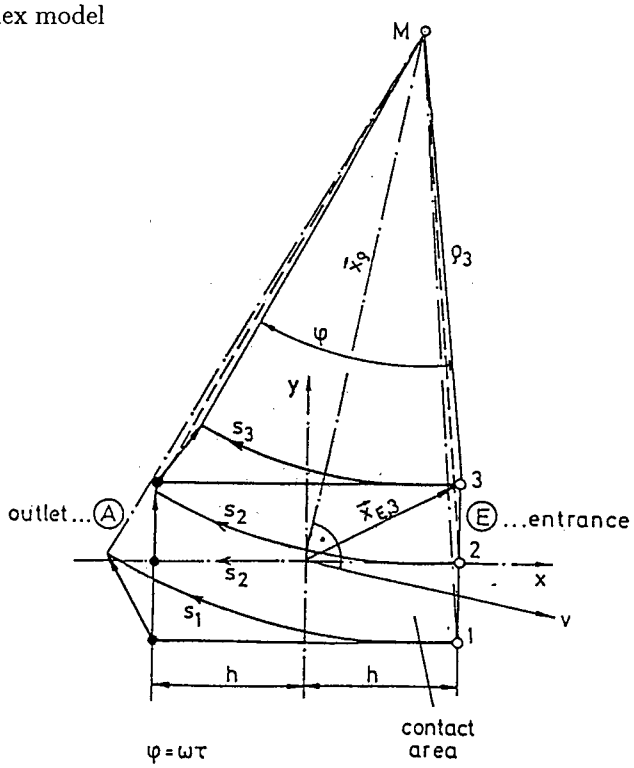

Fig. 6. Stationary rolling of a deformable cylindrical surface: local deformations when the equator line (2) has no longitudinal slip

2. Non-Holonomic Rolling Condition for 2-Dimensional Contact

We begin with the first statement. The non-holonomic rolling condition in this contact area can now be formulated by the idea that we have two

reference planes which are moving one on another. The basic plane x_0, y_0 is the road and the moving plane x, y is oriented by the intersection line of the wheel plane with the road plane. On this line is laying the idealized contact point i.A, which is the intersection of the steepest descent line with the road plane.

Looking for bodies and surfaces with small deformation in normal contact we find only a cylinder on a horizontal plane rolling with horizontal axis or a cone on a cylinder, *Fig. 4*. For both cases there exists in the surface x_0, y_0 there exists a point M around that point the wheel is turning. So we can use this simplified geometry to define the real contact in case of very small deformations. A small flattening of the wheel can be used to define very small tangential deformations $u(x,y)$ and $v(x,y)$ in the moving plane x,y. We distinguish between small, 'local' deformations $\Delta_x(x,y), \Delta_y(x,y)$ and 'global' deformations (for instance lateral bending or eigenmodes) of the wheel $k_x(x,y)$ and $k_y(x,y)$, see *Fig. 5*.

$$\begin{aligned} u(x,y) &= k_x(x,y) + \Delta_x(x,y), \\ v(x,y) &= k_y(x,y) + \Delta_y(x,y)\,. \end{aligned}$$

The area of contact must be known from a contact theory or from measurements, also the functions $\mathbf{k}$ and $\boldsymbol{\Delta}$

Because of the fact that the two planes have a common point M which is not moving in both planes we can formulate the non-holonomic rolling condition:

$$e_\rho(\mathbf{x}) \cdot d\mathbf{x} = 0\,.$$

At first we look for the movement of a contact point in the plane x,y when it is *fixed* in the plane x_0, y_0, see *Fig. 5*:

$$\mathbf{x}_0 = \mathbf{a} + \mathbf{x} = \text{const!}$$

In the moving system x,y we get by aid of the Euler equation:

$$\mathbf{v} + \dot{\mathbf{x}} + \boldsymbol{\omega} x \mathbf{x} = \mathbf{0}\,.$$

From this we get the differential equation:

(*) $$\boxed{\dot{\mathbf{x}} = \mathbf{A}\mathbf{x} + \mathbf{f}}$$

the matrix $\mathbf{A}$ and vectors $\mathbf{f}, \mathbf{x}$ are

$$\mathbf{A} = \begin{pmatrix} 0 & \omega \\ -\omega & 0 \end{pmatrix}, \quad \mathbf{f} = \begin{Bmatrix} -v\cos\delta \\ v\sin\delta \end{Bmatrix}, \quad \mathbf{x} = \begin{Bmatrix} x \\ y \end{Bmatrix}.$$

If all parameters are constant $(\omega_0 v_0 \delta_0)$ the solution consists of circles

$$\mathbf{x}_{(t)} = \mathbf{D}_{(t)}(\mathbf{x}_{(t_1)} - \mathbf{x}_\rho) + \mathbf{x}_\rho\,,$$

where $\mathbf{D}_{(t)} = e^{\mathbf{A}_0(t-t_1)}$, $\mathbf{x}_\rho = -\mathbf{A}_0^{-1}\mathbf{f}_0$. Expanding $e^{\mathbf{A}_0(t-t_1)}$ one finds:

$$\mathbf{D}_{(t)} = \begin{pmatrix} \cos\varphi & \sin\varphi \\ -\sin\varphi & \cos\varphi \end{pmatrix}, \quad \varphi = \omega_0(t - t_1).$$

This solution produces the following field of relative motions, see *Fig. 6.* If the contact points 1, 2, 3 are touching the ground plane at the same time $t_1 = t_E$ and defining the running time in contact by $\tau = t_A - t_E$ the angle φ is for all points 1, 2, 3 the same.

For a differential element of the way of the moving point we get

$$(\mathbf{x} - \mathbf{x}_\rho) \cdot d\mathbf{x} = \mathbf{0}$$

which is a non-holonomic constraint. The location of M is in every case

$$\mathbf{x}_\rho = \left(\frac{v}{\omega}\sin\delta, \frac{v}{\omega}\cos\delta\right)$$

so one gets the constraint equation:

$$\left(x - \frac{v}{\omega}\sin\delta\right)dx + \left(y - \frac{v}{\omega}\cos\delta\right)dy = 0.$$

Multiplying by ω, re-arranging and using the time element dt leads to

$$\frac{dx}{\omega y - v\cos\delta} = \frac{dy}{\omega x - v\sin\delta} = \frac{dt}{1},$$

which defines a family of characteristics. Defining $\mathbf{x} \equiv \mathbf{x}^*(x, y, t)$ as a non-stationary field of moving lines of contact points

$$\dot{\mathbf{x}} = \frac{\partial \mathbf{x}}{\partial x}\frac{dx}{dt} + \frac{\partial \mathbf{x}}{\partial y} \cdot \frac{dy}{dt} + \frac{\partial \mathbf{x}}{\partial t}$$

it follows

$$\dot{\mathbf{x}} = \frac{\partial \mathbf{x}}{\partial x}(\omega y - v\cos\delta) + \frac{\partial \mathbf{x}}{\partial y}(\omega x - v\sin\delta) + \frac{\partial \mathbf{x}}{\partial t} = \mathbf{A}\mathbf{x} + \mathbf{f}$$

which are nonlinear because of $\omega x, \omega y$. It is important to mention here that numerical integration uses time increments Δt and increments $\Delta\psi$, δs_x, Δs_y defined by

$$\Delta\psi = \omega\Delta t, \quad \Delta s_x = v\cos\delta\Delta t, \quad \Delta s_y = v\sin\delta\Delta t.$$

So we get for the new position of the point $\mathbf{x}(t + \Delta t) \equiv \mathbf{x}'$ in all cases, even when $\mathbf{x}_\rho$ goes to infinity (that means pure translation), the following expansions

$\mathbf{x}' = \mathbf{D}(\mathbf{x} - \mathbf{x}_\rho) + \mathbf{x}_\rho = \mathbf{D}\mathbf{x} + (\mathbf{E} - \mathbf{D})\mathbf{x}_\rho$, expanding $\mathbf{D}$ to third order :

$$\mathbf{D} \doteq \begin{pmatrix} 1-\frac{1}{2}\Delta\psi^2, \Delta\psi - \frac{1}{6}\Delta\psi^3 \\ -\Delta\psi + \frac{1}{6}\Delta\psi^3, 1-\frac{1}{2}\Delta\psi^2 \end{pmatrix}, \quad \mathbf{x}_\rho = \begin{Bmatrix} \Delta s_y/\Delta\psi \\ \Delta s_x/\Delta\psi \end{Bmatrix}.$$

$$\begin{aligned} x' &= \left(1-\frac{1}{2}\Delta\psi^2\right)x + \left(\Delta\psi - \frac{1}{6}\Delta\psi^3\right)y - \left(1-\frac{1}{6}\Delta s_x + \frac{1}{2}\Delta\psi\Delta s_y\right), \\ y' &= \left(-\Delta\psi + \frac{1}{6}\Delta\psi^3\right)x + \left(1-\frac{1}{2}\Delta\psi^2\right)y + \frac{1}{2}\Delta\psi\Delta s_x + \left(1-\frac{1}{6}\Delta\psi^2\right)\Delta s_y. \end{aligned}$$

A transformation which is regular, nevertheless if $\tan\delta = \frac{\Delta s_y}{\Delta s_x}$ is small or not. The rotation $\Delta\psi$ must be small, therefore it is necessary to look for the highest frequency of the rolling system with respect to the shannon theorem (for numerical treatment).

The created tangential forces in the contact area are computed in every timestep using the local deformation vector $\mathbf{\Delta}$. With these forces one has to compute the dynamics of the global deformations of the wheel and getting the axle forces of the wheel one computes the dynamics of the vehicle masses. So one gets for the next timestep v, δ, ω.

The local deformation vector is in every case an approximation. As it is the difference between $\mathbf{x}$ and $\mathbf{k}$ it is an engineering judgement. For instance if we say that the idealized wheel is flattened without deformation (cylinder or cone surface without bending resistance) there is the only global vector for the cases a) and b) of *Fig. 4*:

$$\text{a)} \quad \mathbf{k} = \begin{Bmatrix} x_E - R\Omega\tau \\ y_E \end{Bmatrix}, \quad \text{b)} \quad \mathbf{k} = \begin{Bmatrix} x_E - R\Omega\tau \\ y_E + \frac{h^2-x^2}{2\rho} \end{Bmatrix} \quad \begin{aligned} \tau &= \tfrac{h-x}{v\cos\delta} \\ \rho &= \tfrac{R}{\sin\alpha} \end{aligned}$$

$$\text{with} \quad h \ll \rho\,.$$

In case of small lateral movement $y(x,t)$ of the contact points along $-h \leq x \leq h$, $|\delta| \ll 1$, $|\omega h| \ll 1$ and constant velocity v, we get the well known equation of B.v. Schlippe, R. Dietrich:

$$\frac{\partial y(x,t)}{\partial x}(-v) + \frac{\partial y(x,t)}{\partial t} = -\omega x + v\delta\,.$$

This equation was then solved by Smiley using power series in time.

Starting again from first formula $(*)$ and changing to integral equations one may use a Picard iteration with τ as the running time of the point x:

$$\mathbf{x}_{\nu+1} = \mathbf{x}_E + \int_0^\tau (\mathbf{A}\mathbf{x}_\nu + \mathbf{f})d\tau\,,$$

and beginning with straight line running of every point

$$\mathbf{x}_1 = \mathbf{x}_E - \mathbf{e}_x R\Omega\tau \quad \text{with} \quad \tau = \frac{h-x}{v\cos\delta}\,,$$

we find for a cylindrical wheel with small lateral deformation $y(x,t)$

$$y(x,t) = y_E(t-\tau) + \int_0^\tau (v\delta - \omega x)d\tau$$

a first iteration.

By definition $d\tau = -\frac{dx}{v_x}$ and $v_x \doteq v = R\Omega$ (no longitudinal slip) we get the differential form:

$$y(x+dx,t) = y(x,t-d\tau) + (v\delta - \omega x)d\tau\,.$$

Expanding this to first order

$$y(x,t) + \frac{\partial y}{\partial x}dx = y(x,t) - \frac{\partial y}{\partial t}d\tau + (v\delta - \omega x)d\tau\,,$$

dropping $d\tau$:

$$\frac{\partial y}{\partial t} - v_x\frac{\partial y}{\partial x} = v\delta - \omega x$$

which shows, that this type of equation is only a first approximation.

3. Dynamics of Real Wheels Using Continuum Theorie

For technical applications the contact points are not only sticking on the surface of contact they are also slipping when the friction limit for a given pressure distribution is reached. To simplify the model in these cases the velocity of sliding is computed only using the rotation velocity and vibrational velocities of the eigenmodes of the wheel. The local deformation velocity is neglected. So only low frequency self excited excitation is possible. Because of decrease of the friction function with increasing sliding velocity a dynamic rolling stability problem arises: stiction forces and friction forces are nonconservative and so there is a need to get energy losses into the wheel body to stabilize the fast rolling system.

Looking through a running glass plate for the contact behaviour of the points is contact area, see *Fig. 7*, and estimating the moving of white points which are labelled on the surface of the tire and using image processing for instance fir a rolling situation of five degrees of slip angle one sees, see *Fig. 8* that in front of the contact area the points are sticking and later on they are slipping. This behaviour was also computed, see *Fig. 9*, using two lateral

eigenmodes of the wheel, local shear deformation behaviour of the profile elements and given pressure distribution. The area of contact is assumed to be a section of the toroidal shaped tire surface. To increase rolling stability the eigenmodes must be damped.

Finding by resonance excitation for the first two lateral eigenmodes of the tire where the damping is placed, it was found that it is mostly damped in the sidewalls, which can be shown by thermography, see *Fig. 10.* Also the friction behaviour of the profile elements produce damping, which was computed and controlled also by thermography, see *Figs. 11* and *12* and the computed tire forces are also controlled by sinusoidal excitation of the steering angle running the tire on a drum. Reaching the flutter point of the tire at a wavelength of one meter there is shown a ninety degree phase lag in the *Fig. 13.*

Longitudinal and lateral oscillations with higher frequency of the profile elements were introduced into the system by OERTEL who has shown the influence of friction oscillation of the profiles on the generated tangential contact forces (increasing roughness).

4. Dynamics of Rolling Wheels with Non-Smooth Surface

A further discretisation of the whole wheel and of the contact elements was made using particle dynamics. So it was possible to compute simultaneously global deformations, local deformations, pressure forces, see *Fig. 14* and *15*, and friction forces. A non-holonomic constraint equation is not used. There is only used a holonomic constraint equation when a particle is touching the ground. It is assumed that it is sticking in the first time step when touching the ground because there is no tangential local deformation. In the next time step it is proved if it is sliding or not. Naturally one has a high frequency system of particles and one has to use a very short time step for integration.

Lastly the footprint of the tire was computed, see *Fig. 16*, and it was compared with thermographic estimated footprint see *Fig. 17.* So we end with this research, looking for the high-frequency behaviour in contact area up to 2000 Hz, producing solutions and measurements of this behaviour but do not use non-holonomic constraints again, which was done at a first attempt as a good working hypothesis, and later on looking for nonsmooth surfaces the practicability was bad. Going into the details of the profile deformation discretization is always necessary, but we have to be aware of the fact that we lose a possibility of analytical treatment. But otherwise, to understand all phenomena which occur in the contact region, it is necessary to develop complex numerical models for the behaviour of rolling wheels.

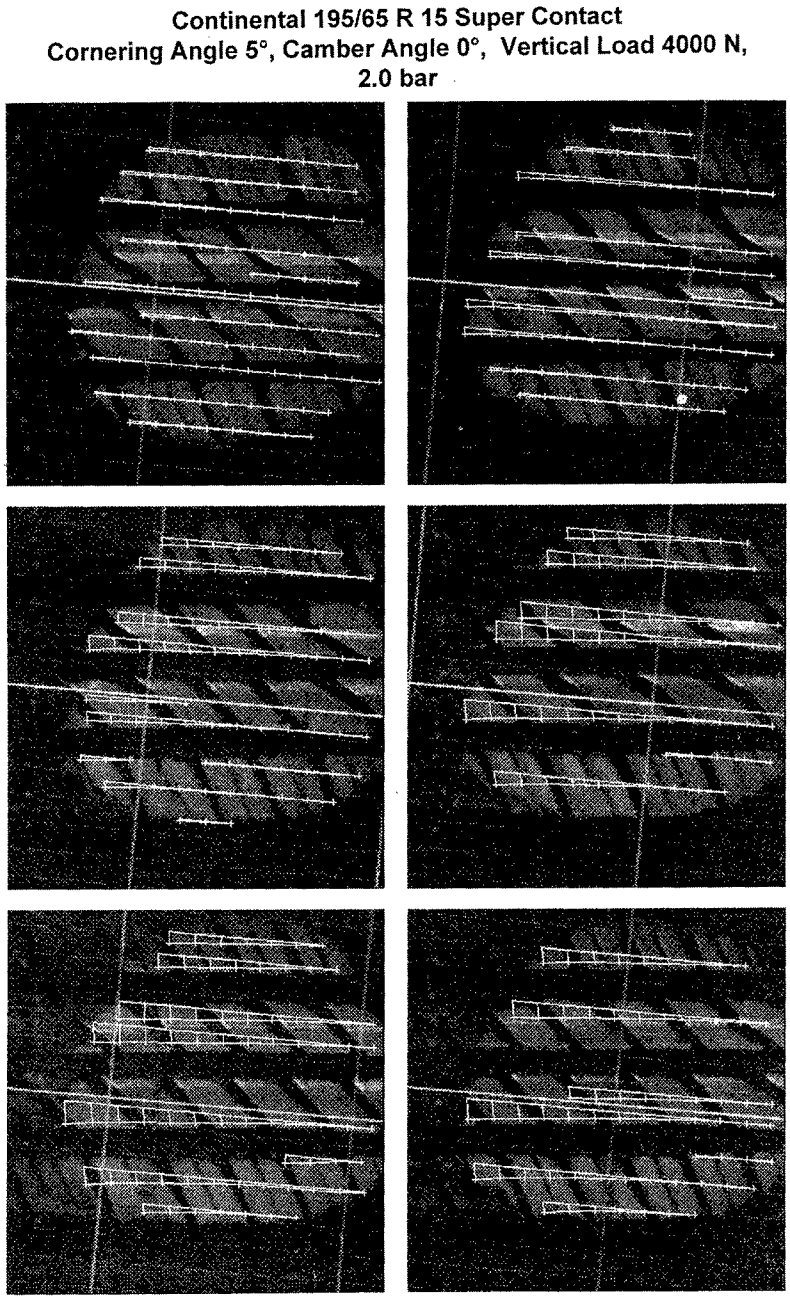

Fig. 7. Tire rolling nonstationary on a glass-plate beginning from upper left to right down : white marked points on the profile elements show the movement relative to inclined motion ($\delta = 5°$) of the plate. At the entrance the points move with the same angle, then they slide laterally, velocity is $v = 2.5$ cm/s.

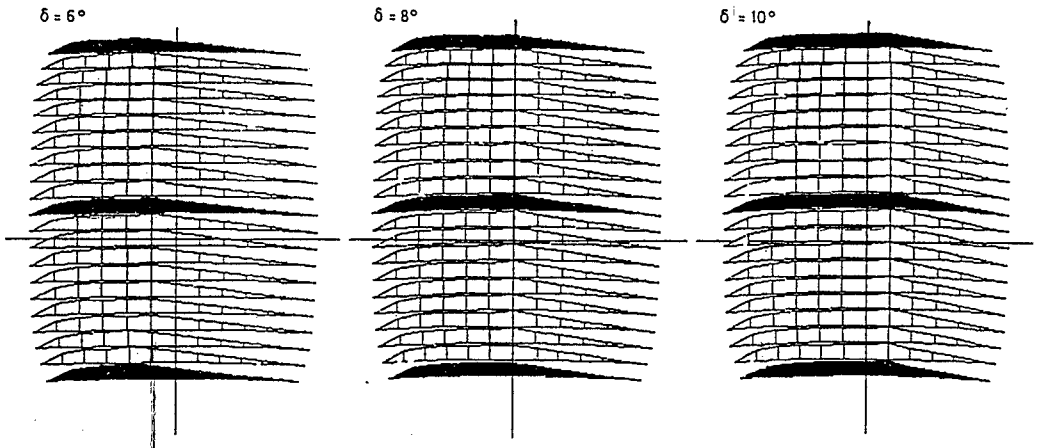

Fig. 8. Computation of rolling situation with $\delta = 6°, 8°, 10°$ using 21 lines and 13 collocation points on every line

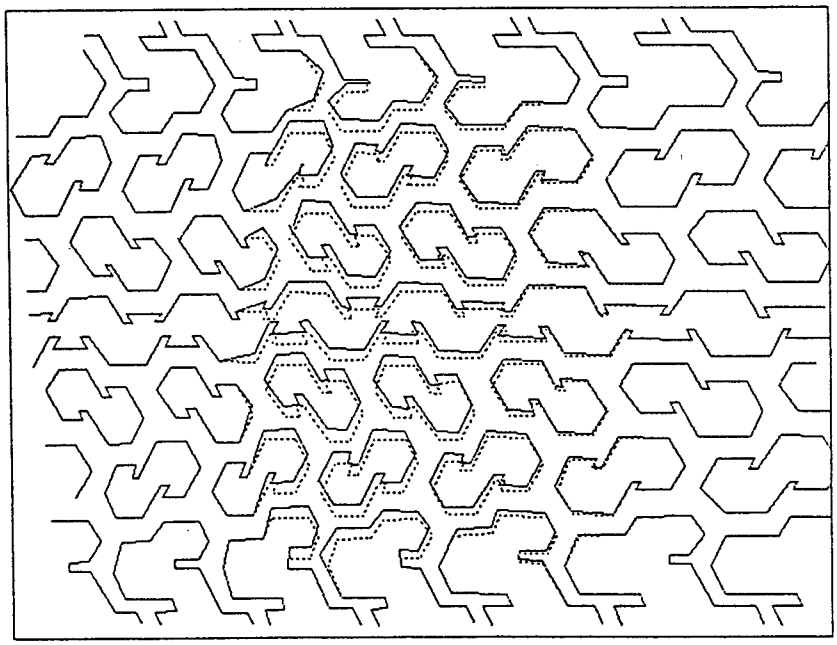

Fig. 9. Local deformation computed for $\delta = 5°$

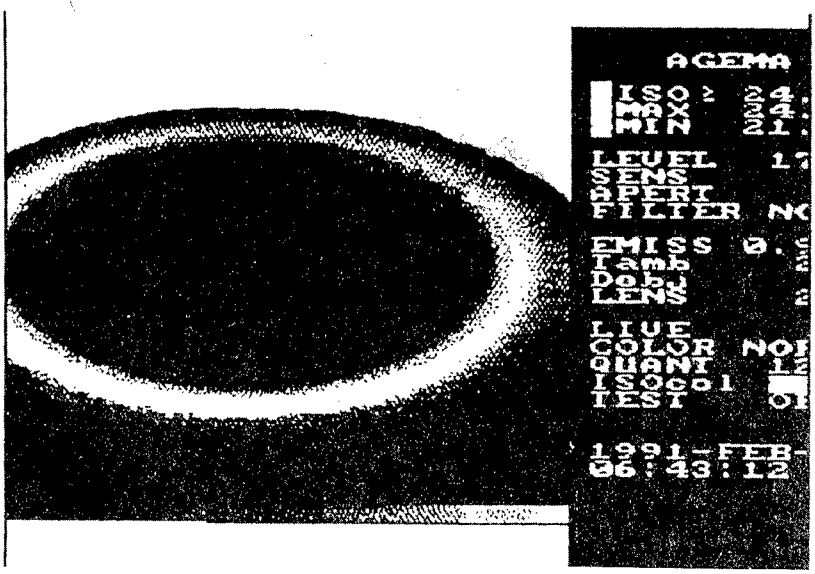

Fig. 10. Eigenmode $n = 0$ for lateral excitation of the tire

Fig. 11. Thermography of frictional heat up of the slipping profile elements, concerning angle 5°, camber angle 5°, vertical load 3000 N

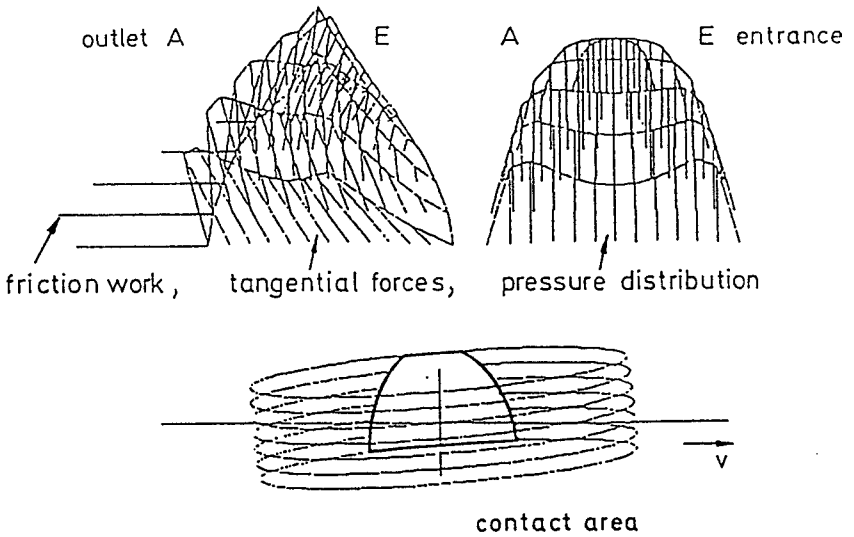

Fig. 12. Computed results of friction work, tangential forces and pressure distribution, stationary rolling

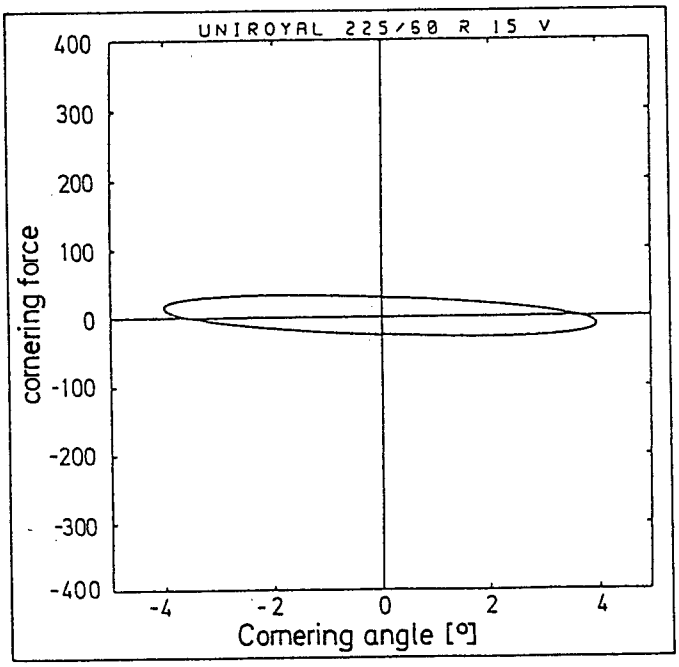

Fig. 13. Computed flutter point for a 225/60 R 15 V tire

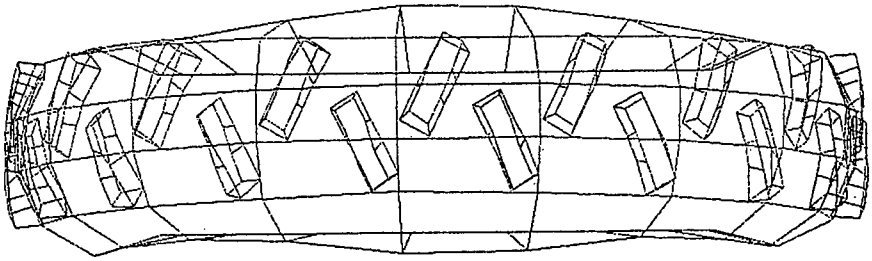

Fig. 14. Computed deformation of a tire model with profile elements, cornering angle 5°, load 3000 N

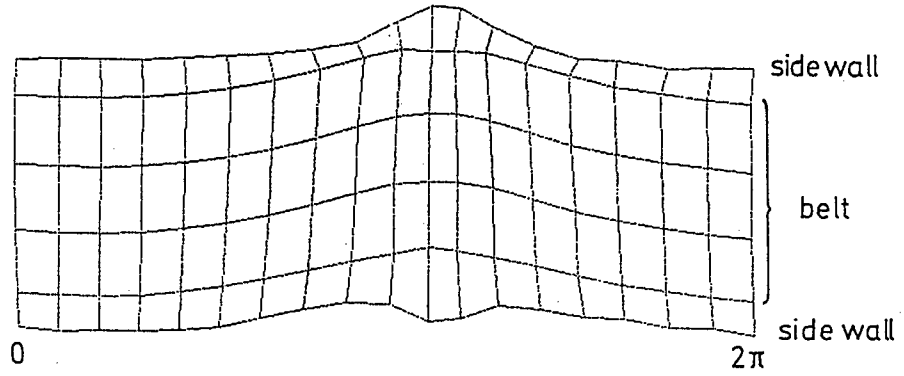

Fig. 15. Computed lateral deformation of the tire carcass

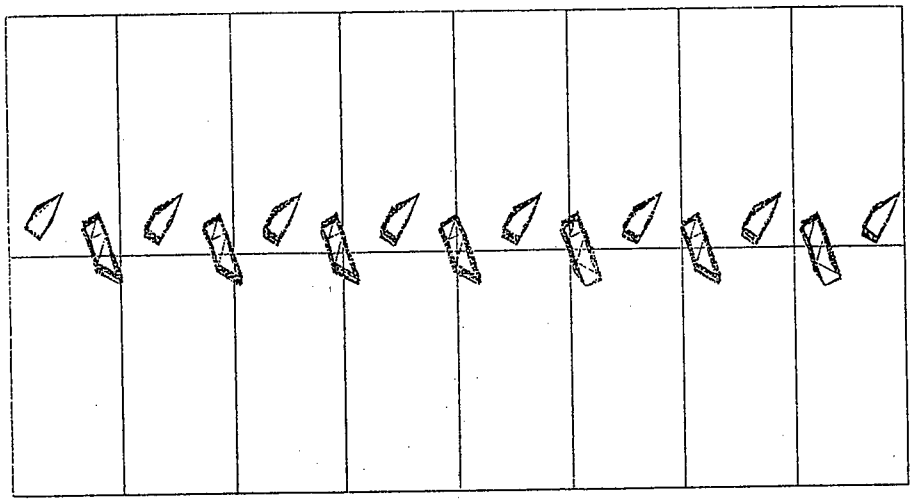

Fig. 16. Computed footprint of model on a plate

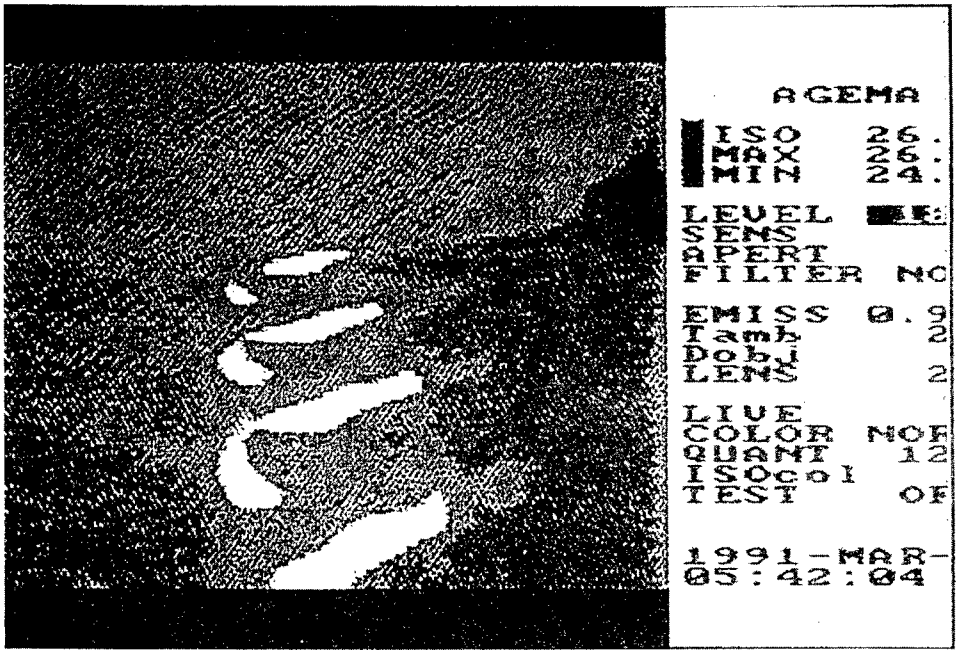

Fig. 17. Thermography of a rolling tire with this profile on a flat bed test rig, cornering angle 5°

Conclusion

The concept of a non-holonomic condition for a single contact point was the first step into dynamics of vehicles. The next step was to extend the concept to a contact line and to a contact area.

Introducing a friction law big problems arise: there is no theory for friction oscillations in continuum theory. But for discrete systems it was possible to produce correct and stable numerical solutions. So it was shown that high frequency behaviour of rolling wheels always needs an engineering decision what eigenmodes have to be used.

Rolling and slipping of real wheels can only be simulated numerically using particle dynamics. Computing the contact of the surface particles touching the ground, it is necessary to use holonomic constraints. The frequency range of the solution is limited to avoid excessive computing time.

Appendix 1

$$\begin{aligned} m(\dot{v}_x - \omega v_y - \omega^2 a) &= 0, \\ m(\dot{v}_y + \omega v_x + \dot{\omega} a) &= R, \\ I_s \dot{\omega} &= -Ra, \end{aligned}$$

$$0 < v_x = \text{const.}\,, \quad v_y = \dot{v}_y = 0\,, \quad \dot{\psi} = \omega,$$

$$m(\omega v_x + \dot{\omega} a) = -I_s \frac{\dot{\omega}}{a},$$

$$\boxed{\dot{\omega} + y\omega = 0}\,, \qquad \lambda = \tfrac{mav_x}{I_s + ma^2},$$

$$\left\{ \begin{array}{ll} \text{stable}: & a > 0 \\ \text{unstable}: & a < 0 \end{array} \right\} \quad \text{solution} \quad \omega = \omega_0 e^{\lambda t}$$

Appendix 2

$$\mathbf{v}_E = \left\{ \begin{array}{c} v \\ -v\delta + h\omega \end{array} \right\} + \left\{ \begin{array}{c} 0 \\ \dot{\psi} L \end{array} \right\} + \left\{ \begin{array}{c} -v \\ v\psi \end{array} \right\} \doteq \mathbf{0}$$

$$\rightarrow v\psi + h\omega + L\dot{\psi} - v\delta = 0$$

$$\psi = \frac{y_E}{L}\,, \quad h\omega \approx 0 \quad \left(h \ll \rho = \frac{v}{\omega}\right),$$

$$\dot{y}_E + v\left(\frac{y_E}{L} - \delta\right) = 0\,, \quad c_S y_E = S,$$

$$S = c_S L\left(\delta - \frac{\dot{y}_E}{v}\right) = c_S L \rho_{\text{eff.}},$$

$c_S L \ldots$cornering stiffness,

$$M \doteq \frac{1}{3} hS \quad \text{(linear distribution)}$$

References

[1] BÖHM, F.: Theorie schnell veränderlicher Rollzustände für Gürtelreifen, *Ingenieur-Archiv*, Vol. 55 (1985) pp. 30–44.

[2] BÖHM, F.: Einfluß der Laufflächeneigenschaften von Gürtelreifen auf den instationären Rollzustand, DKG-Tagung, Mai 1987 in Wien (Österreich).

[3] KMOCH, K.: Meßtechnische Methoden zur Bewertung dynamischer Reifeneigenschaften, Dis. 1992, TU Berlin.

[4] OERTEL, C.: Untersuchung von Stick-Slip-Effekten am Gürtelreifen, Dis. 1990, TU Berlin.

PERIODICA POLYTECHNICA SER. TRANSP. ENG. VOL. 24, NO. 1, PP. 65–80 (1996)

MODERN CONTROL THEORY APPLIED TO VEHICLE DYNAMICS

STATE-OF-ART REPORT

József BOKOR* and László PALKOVICS**

* Computer and Automation Institute of the
Hungarian Academy of Sciences (SZTAKI)
H–1111 Budapest, Kende u. 13–17, Hungary
** Department of Automobiles
Technical University of Budapest
H–1521 Budapest, Hungary

Received: 9 November, 1994

Abstract

This paper gives a state-of-art report of the controlled vehicle dynamical research that has been conducted at the Technical University of Budapest and the Computer and Automation Institute of the Hungarian Academy of Sciences. The investigations into the application of the newest results of the modern control and identification theories are conducted on several fields: primary (wheel) suspension control, secondary vibration isolation (seat), steering systems, control of the hitch forces and torques at articulated vehicles, and stability enhancement control systems. There are some other fields addressed here as well, which are related to the interface between the vehicle and the environment (IHVS) and the investigations into the on-board vehicle electronics.

Keywords: modern control theory, robust control, automated vehicle systems, vehicle dynamics, identification of dynamical systems.

1. Introduction

With the sharply increasing number of the vehicles participating in the everyday traffic several other factors receive a growing interest:

- risk of traffic accidents, which is not only the consequence of the number, but also the higher performance of the vehicles,
- the need for increasing the traffic flow's velocity and safety,
- demands on the better communication between the vehicle, vehicle driver and the environment.

The above facts are pointed out very clearly that the vehicles of the end of 20th century should be smart and have a certain intelligence to fulfil all these requirements. It basically means significant increase in the job of the on-board computer. Its task will be changed essentially: it should not only communicate with the existing electronic system and control their behaviour (such as engine management, ABS, climate control, etc.) but also should

handle complex problems such as vehicle identification, controller design, communication with the road properties (curvature, elevation, etc.) linked to a satellite communication system. The principal scheme of such a vehicle can be seen in *Fig. 1.* In this state-art-of report only the results related to some of the controlled dynamical systems installed on the vehicle are introduced. In the reference list, a completer picture about the publication activity conducted in this field is given [1]–[15].

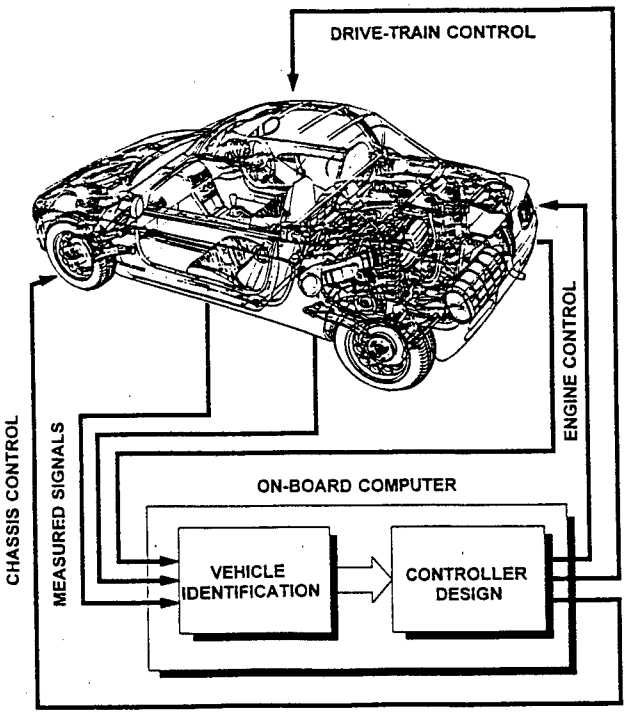

Fig. 1. General task of the on-board computer

2. General Problem Statement

Generally speaking, any controlled dynamical system can be transformed into the form shown in *Fig. 2*, which gives the basis for the controller design.

There are three blocks in *Fig. 2.* The middle one represents the nominal plant to be controlled by the lower block, which is standing for the controller. Since the real systems cannot be known perfectly (there are several facts making the system uncertain), the upper block describes the model of system's uncertainties. These can be structured (such as the physical parametric uncertainties) or unstructured (arising from high order or non-

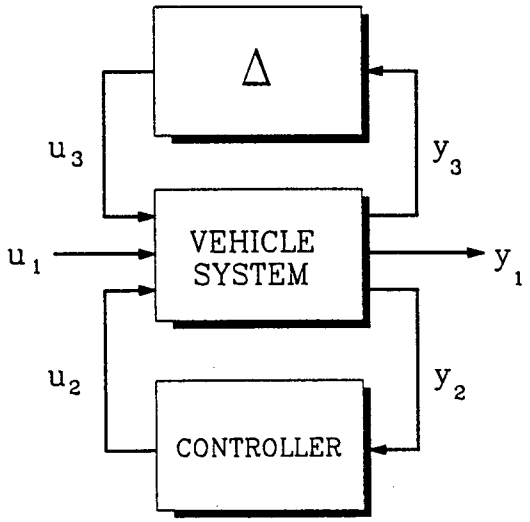

Fig. 2. Block diagram of an uncertain dynamical system

linear dynamics). The input vector $\boldsymbol{u}_1$ stands for the external disturbances acting on the system, $\boldsymbol{u}_2$ is the control input vector. The set of outputs denoted by $\boldsymbol{y}_1$ is referred to as the performance output vector which has to be controlled, and $\boldsymbol{y}_2$ contains the measurable outputs.

In vehicle dynamics, several classes of models can be used. As a first approach to the controller design problem, linear time-invariant (LTI) models are used, and thean, when implementing it in highly non-linear environment, the models can be refined with time varying and/or non-linear disturbances and uncertainties. The mathematical system theory offers (a) transfer function models with norm bounded unstructured uncertainties and (b) state-space models with both structured (parametric) and unstructured uncertainties.

In vehicle dynamical studies the system's performance output varies from application to application. For example, in the suspension design problem it contains the vertical body acceleration and the dynamic wheel load, while designing controlled 4WS system, the controlled outputs are the lateral acceleration and the yaw rate. Similarly, the control inputs are also different, in the suspension case it is a force, while at the 4WS system it is the steering angle. These variables will be mentioned later at the specific application. When talking about integrated vehicle control as shown in *Fig. 1*, these output and input signals are collected into one vector and are used in control.

Generally speaking, the control problem can be formulated as follows:

$$\|\boldsymbol{T}_{\boldsymbol{y}_1,\boldsymbol{u}_1}\|_A(\boldsymbol{K}\Delta) \rightarrow \min_{\boldsymbol{K}\in k_{stab}} \tag{1}$$

that is some norm of the transfer function between the performance output and external disturbances is minimized over a set of stabilizing controllers. The solution to the control problem given in *Eq.* (1) can be obtained as:

a) H_∞ optimal control or minimax differential game, where the L_2 induced norm is used in *Eq.* (1) and it is assumed that the signals are energy constrained, bounded, i.e. $\boldsymbol{u}_1$ and $\boldsymbol{y}_1 \in L_2$.
b) l_1 optimal controller design: it is assumed that the signals are amplitude constrained, i.e. $\boldsymbol{u}_1$ and $\boldsymbol{y}_1 \in L_\infty$ and the norm in *Eq.* (1) is the induced L_∞-norm.
c) H_2/H_∞ design problem (see in [11], [12]), when $\boldsymbol{u}_1(t)$ is stochastic and Δ is norm bounded.

The design steps can be listed as: (a) construct the equations of motion, (b) convert it into the state-space form and $M - \Delta$ form (this is form when the plant and controller block in *Fig. 2* are combined into a single M block) and (c) depending on the control goal choose the right algorithm to synthetize the controller. The controller design problem can ususally be solved by a commercially available software, such as MATLAB or MATRIX$_x$. If the model cannot be obtained from e.g. first principle, system identification has to be performed prior to the controller design.

3. Suspension Control

In this part of the paper three suspension related problems will be addressed: active and semi-active control of the primary suspension of a passenger car, and the seat suspension design for heavy commercial vehicles.

3.1. Active Suspension Design

Fig. 3 shows the well known quarter-car vehicle model (representing the quarter of the vehicle body with a single suspension), which is widely used for active suspension design because of its simplicity, low number of state variables and parameters. The model is drawn similar to *Fig. 2.* The performance output vector contains the following variables to the controlled (see in references [4], [6], [11], [12]):

- *Vertical body acceleration*, which describes the ride comfort provided by the suspension. This quantity should be minimized in some frequency ranges, because the human body (driver, passenger) is sensitive to vibration transmitted from the road profile to the vehicle in a given frequency range.

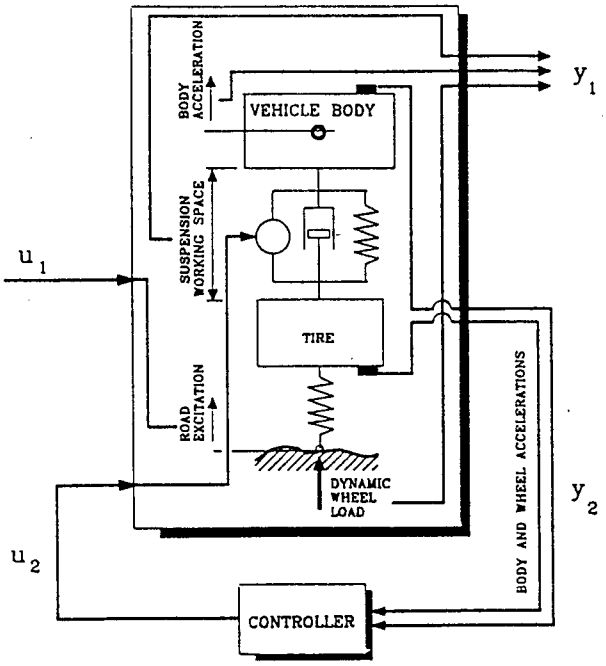

Fig. 3. Quarter-car vehicle model for active suspension design

- *Dynamic wheel load*, whose value should also be kept as minimal as possible to provide better road holding for the vehicle, increasing its lateral and longitudinal stability.
- *Suspension working space*, which is important to be as low as possible, since the large working space causing higher variation in the steering geometry is not permitted from constructional point of view.

The above described quarter-car model is not able to take several effects into consideration: effect of the pitch and roll motion, chassis flexibility, etc., but provides very good results for the theoretical investigations, testing several control schemes. This model can also be uncertain, since such variables as tire spring stiffness (which is a function of internal tire pressure) or the vehicle mass (varying with the number of passengers, or the cargo) are not perfectly known. The approach introduced in part 2 is able to handle such structured uncertainties. The solution to the combined H_∞/RLQR (Robust Linear Quadratic Control) is shown in *Fig. 4* (for more details see in [4], [12]).

Although the simulation results have shown the applicability of the developed control strategies, it should also be implemented in a physical model. For this reason, a 1 : 1 scale quarter car test rig was designed, as shown in *Fig. 5*.

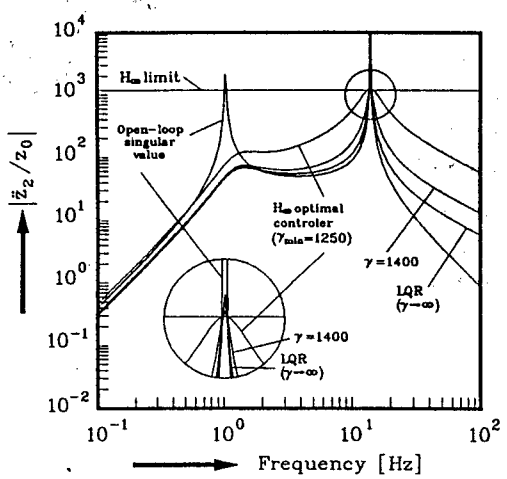

Fig. 4. Transfer functions with different control strategies

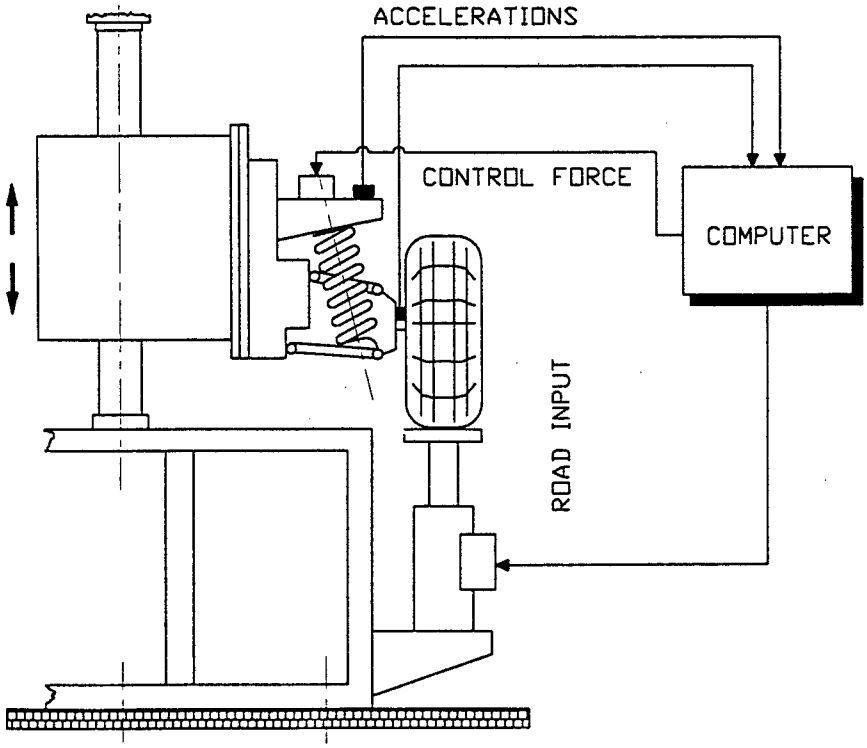

Fig. 5. Quarter-car model test rig

The vehicle body is represented by a vertically moving mass, onto which a two-arm front suspension is attached, keeping the original geometry

of the suspension. The linear bearing needed a special attention because of the friction problems. The road excitation is generated by a Rexroth servo cylinder with maximum capacity of 25 kN (compensated for 15 kN lateral force) and bandwidth of 60 Hz. As active element, a 10 kN, 70 Hz servo cylinder is used, especially manufactured for this application and fitted into the suspension's coil spring replacing the shock absorber. Two accelerations are measured, one is on the body, the other on the lower wishbone. The system will be controlled by a PC based DSP board.

Although the results obtained from this investigation are promising, there are several factors putting strong limitation on the applicability of the fully active suspension:

- the cost of the active suspension's components (valves, cylinders, power supply, etc.) is very high, and makes it very expensive for the customer.
- the energy demand of the system (producing large oil flow and pressure) is very high and should be generated by the car engine, which results in a loss of the accelerating performance, decrease of the maximum speed.

These two facts explain that not too many car producers are dealing with active suspension development for serial production. However, there are some special vehicles where their application is feasible: transporting expensive goods (e.g. vibration sensitive instruments, computers) or systems (for example military command points with high speed).

3.2. Investigation of Semi-Active Systems

As it was pointed out at the end of the last paragraph, the active suspension system is not really feasible from point of view of the high energy demand. This problem can be eliminated by replacing the fully active actuator by a semi-active one. The semi-active actuator is a variable damping-coefficient shock absorber, which is able to vary its damping ratio with high bandwidth. The semi-active damper is able to dissipate energy only, but in a controlled way. The system's model is similar to the active suspension shown in *Fig. 3*, only the actuator is replaced by a controllable damper, and the control strategy should be modified. The derivation of the continuous as well the discrete semi-active control strategy is shown in *Fig. 6.*

As seen in *Fig. 6.a*, with the active control any relative velocity between the vehicle body and wheel can be controlled. The ideal semi-active damper should be able to generate zero and infinite damping coefficient, but only energy can be dissipated (*Fig. 6.b*). Since neither zero nor infinitely large damping ratio can be obtained, the control range in the 1st and 3rd quarter is narrowed (*Fig. 6.c*). The continuous system operates fine, but this is more

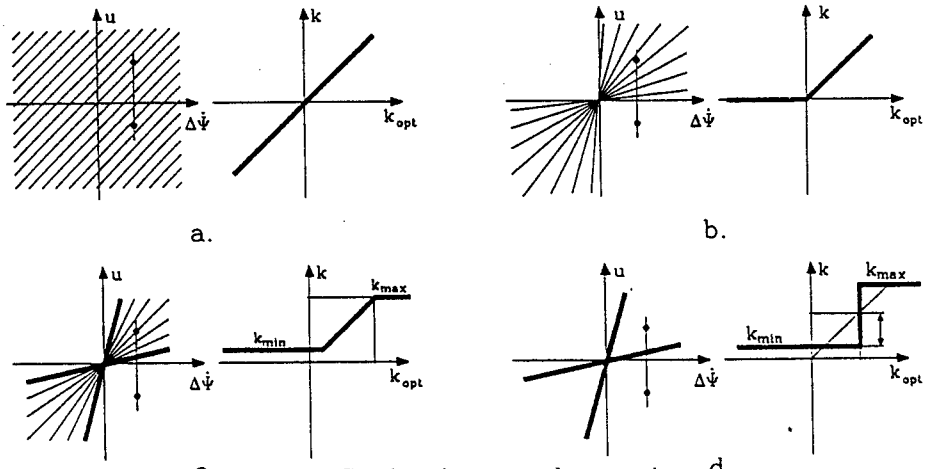

Fig. 6. Semi-active control strategies

expensive, since it needs more complicated hardware. That is why usually a two, or more stage damper is for semi-active suspension control. In *Fig. 6.d* a two-stage semi-active damper control logic is shown.

The semi-active suspension control project was conducted together with the Vehicle Research Laboratory of the Delft University of Technology, the Netherlands. Using the vehicle, fitted with controllable dampers at the rear, some of the measured results can be seen in *Fig. 7.* The figure shows measurements at the low-damper stage (about 300 Ns/m), high damper stage (about 900 Ns/m) and with the semi-active damper. As seen in the upper chart of *Fig. 7*, with low setting the peaks at about 1 Hz and 11 are high, the low damping results in large amplitude at the eigenfrequencies of the vehicle, while in the frequency range of 4–9 Hz the gain is low. With high setting it is in opposite, the peaks are eliminated, but there is large gain in frequency range of 4–8 Hz, where the human body is more sensitive to the vibration. With semi-active damper control (SAD) the optimum between these two limits can be found. However, two problems can be detected: (a) the improvement is not too large, which is caused by the small difference between the low and high damper settings, and (b) undesired oscillatory motion can be seen in higher frequency ranges. This last phenomenon, referred as chattering, is inherent problem of variable damper systems. Some solution to eliminate this vibration can be found in [2]–[11] using sliding mode control.

However, the semi-active suspension system is getting more widely used, all the leading car manufacturers offer this system for the products.

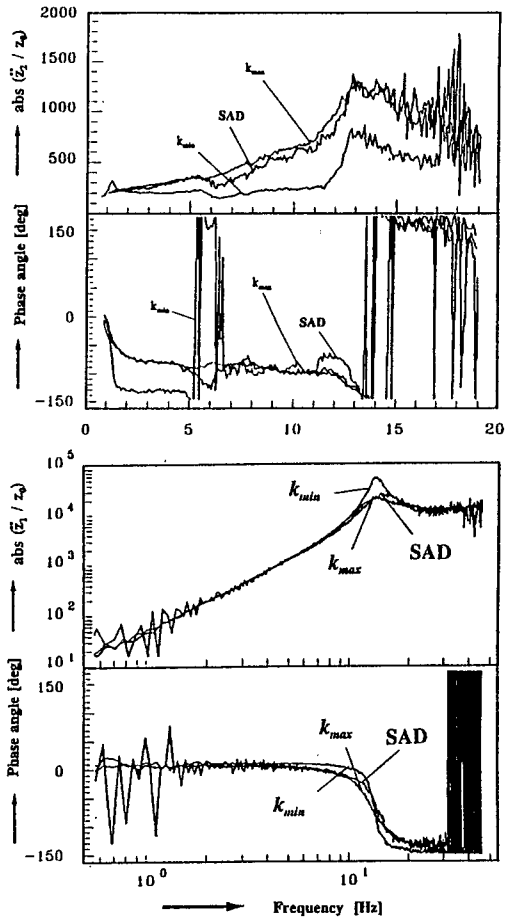

Fig. 7. Transfer functions between the body and wheel accelerations and the road excitation (measured results)

3.3. Controlled Seat Suspension Design

In heavy vehicles primary suspension controlled elements usually cannot be applied, because of high loads, which should be carried by the controlled actuators. The modification of the suspension itself is sometimes also not possible. However, the heavy truck drivers are subjected to a logn term vibration, whose effect is prolonged during their lifetime and might result in serious illness requiring millions for medical treatment, hospitalization, rehabilitation, etc. Similar problem can be found in other type of vehicles, such as agricultural tractors, mining vehicles, where the primary suspension is very stiff (if exists at all).

In this case the driver's seat suspension can be modified to give better isolation fot the driver. This type of activity has been started recently, and some very first results have already been published (see in [2, 10]). *Fig. 8a* shows the model of a combined human-driver and quarter-vehicle.

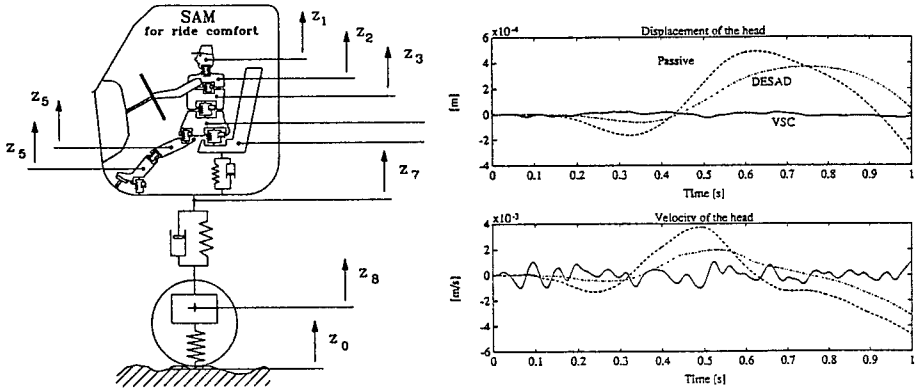

Fig. 8. (a) Combined model of a human driver and vehicle
(b) Some results with sky-hook controller

In this case similar control problem is solved as introduced before. The driver's seat is suspended by using a semi-active damper. The control strategy is designed based on the so-called 'sky-hook' principle, which means that the damper's switching algorithm is working similar to a damper installed between the seat and an inertial reference point (the 'sky'). When the required sky-hook force is having the same sign as the one can be produced by the shock absorber, the high stage is set, when the sign is opposite, the low stage is set. By applying this control strategy, some of the results can be seen in *Fig. 8.b.*

The results prove the applicability of this procedure. Recently, a practical realization of this theoretical investigation has been started. A heavy truck seat's suspension will be modified, applying the same actuator as for the active suspension model, and another servo cylinder is used to generate the vehicle floor excitation, based on a real vehicle's motion on a given road profile.

The driver seat suspension control is not a new topic for investigation, some adaptive systems can also be bought. These seats usually have pneumatic suspension, which varies the internal air-pressure according to the driver's weight, the road roughness, etc.

4. Stability Control

The other field of control application investigated by TUB and SZTAKI is vehicle lateral control, although beyond a certain point (integration of different control systems in order to achieve better performance, optimal sensoring) they cannot be separated. Three different fields are being investigated here: the potentials of the four-wheel steering (4WS), controlled anti-jackknifing systems, and stability enhancement control for combination vehicles (such as car–caravan combinations, articulated buses, and heavy vehicle configurations).

4.1. Four-Wheel Steering Systems

The control logic of the 4WS system can be drawn into the block scheme in *Fig. 2.* As seen in *Fig. 9*, the external inputs to the vehicle system are the driver's steering angle, expressing his intention, and a side disturbance, arising from side wind, for example. Control goal of the 4WS steering system is twofolded: at low speed to increase the manoeuvrability of the vehicle by steering the rear wheels in opposite to the front ones, while at higher speeds to decrease the vehicle lateral acceleration and yaw rate, avoiding the sliding or spinning-out of the vehicle. The control scheme for this latter case is shown in *Fig. 9.*

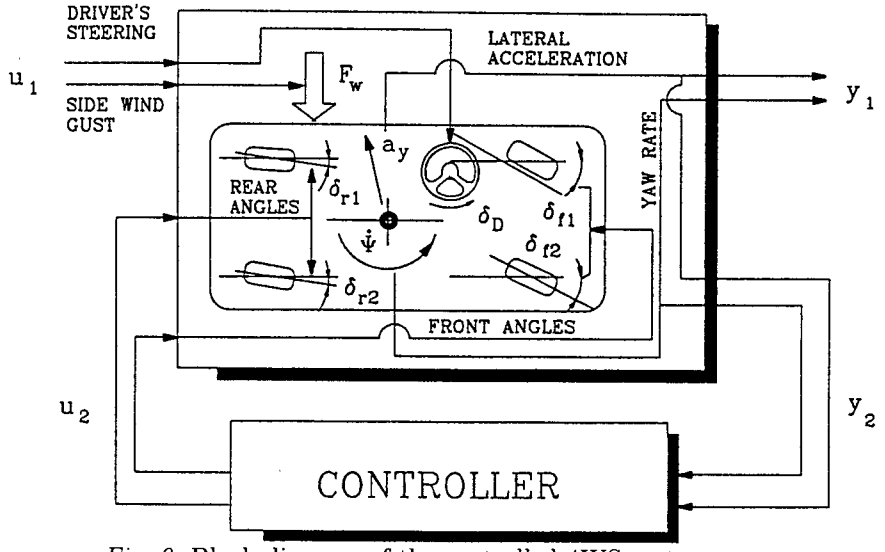

Fig. 9. Block diagram of the controlled 4WS system

The controller design procedure is not as obvious as in the suspension case, since it is not possible to compensate for any perturbation. Although the driver's steering angle is shown as external disturbance, the controller

does not have to attenuate it. There exist several control implementations as well: (a) the one shown in *Fig. 9* is called autonomous control (see in [5]), where the steering wheel is only a sensor, but it is not linked directly to the wheels (b) only the rear wheels are steered only by actuators, the front ones are steered directly by the driver (c) so called additional steering, where the rear wheels are steered actively, the front ones are mechanically, but some correction is possible by actuators.

Additional advantage of the active 4WS systems is the ability of compensating for the lateral disturbances, such as a sudden side wind gust. In this case, possibly without any effort of the driver, the disturbance can be attenuated by only steering of the rear wheels, as shown in *Fig. 10.* This figure shows also the sensitivity of the 4WS system for some physical vehicle parameters (rear axle cornering stiffness). This explains the need for robust control design which was investigated in reference [1].

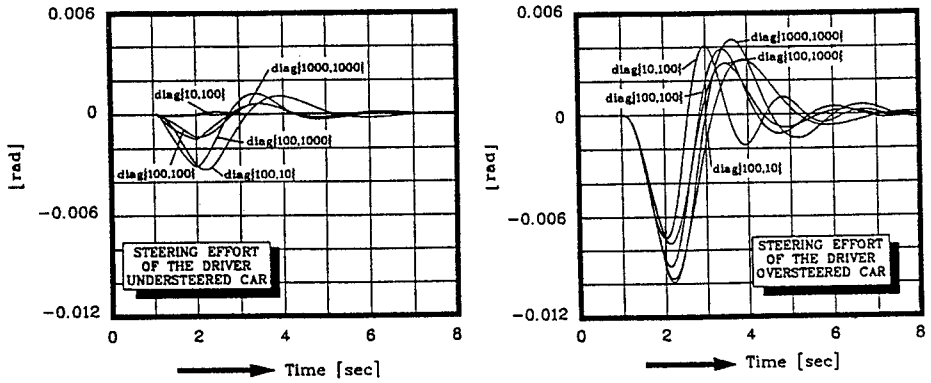

Fig. 10. Compensation for side wind disturbance (a) with the nominal model (b) with uncertain model

4.2. Jackknifing Control in Combination Vehicles

The stability problems of the combination (or articulated) vehicles differs from that of the single vehicles. There are some typical forms of loosing stability for articulated vehicles: roll-overn jackknifing and the self-excited oscillation of the towed vehicle unit. The problem of jackknifing can be found in both tractor–semi-trailer configurations and articulated buses. This is very important consideration in the pusher types (whereas the engine is located at the second unit, and the third axle is driven), since the traction force produced by the tires on the third axle is transmitted to the front through the fifth-wheel. When the front and rear units' angle is larger,

there is a considerable force acting on the hitch in lateral direction (see *Fig. 11*), which pushes the second axle out, leading to jackknifing. In this type of the vehicle this is normal phenomenon, which should be hindered. However, jackknifing can occur in tractor–semi-trailer vehicles especially when braking on slippery road. To avoid the jackknifing in this case the ABS helps a lot until a certain point, but the physical limits cannot be overcome.

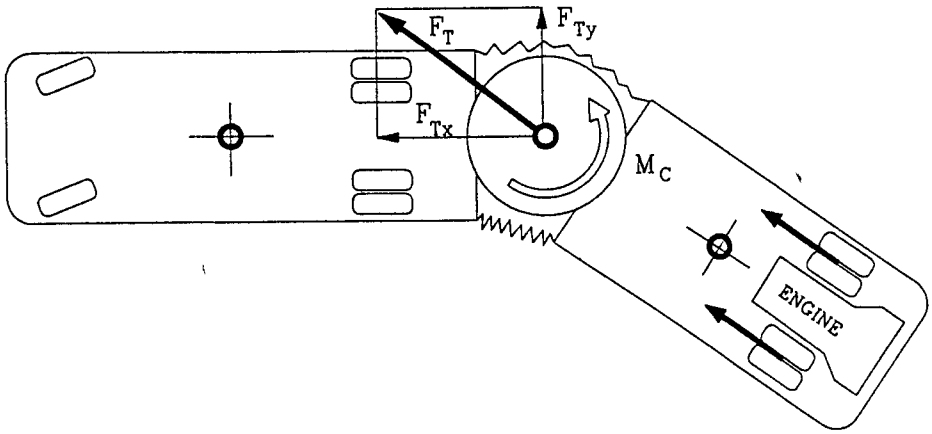

Fig. 11. Hitch moment control for articulated bus of pusher type

The key of controlling such a motion in combination vehicles is the control of the torque M_C in *Fig. 11.* In articulated buses, where the turntable provides enough room, either controllable dampers or large diameter disk brakes are fitted. Both these strategies are semi-active since none of them is able to introduce additional energy, only dissipate it. Beyond a certain hitch angle, both systems are locking and do not allow any larger angle, hindering the jackknifing.

For a tractor–semi-trailer vehicle configuration similar system was investigated in [3]. As was shown, the semi-active hitch torque control has shown improvement in the oscillatory behaviour of the trailer, but it was not able to control the vehicle's roll motion. Furthermore, for tractor–semi-trailer it needs additional devices to be installed making the vehicle price higher at lower benefits.

4.3. Stability Enhancement Control (SEC) of Combination Vehicles

The combination vehicles' stability can considerably be improved by generating a stabilizing yaw torque on the towing vehicle unit. This torque could only be produced by operating the vehicle's brake on one side or on the other. The main advantage of this system is that does not need any

additional actuators and sensors, since the brakes are already installed, yaw rate, acceleration sensors will be a part of the new generation on-board computers installed on the ECU card. This system is described in [3], [7], [8], [13]. *Fig. 12* shows a car–caravan combination with SEC.

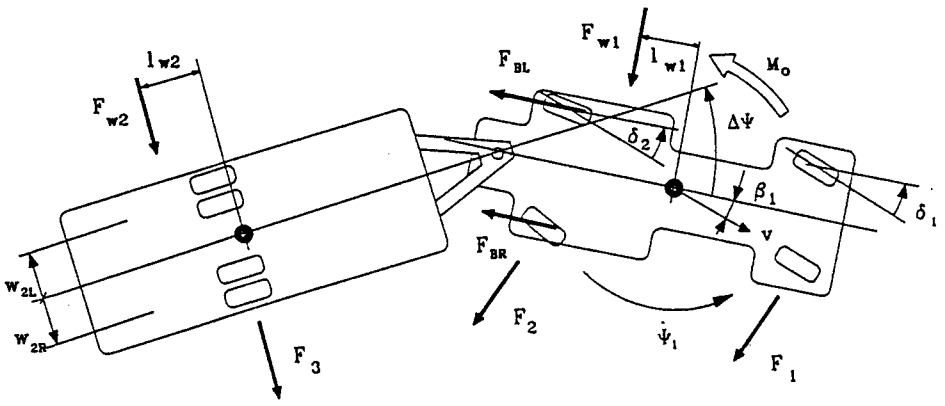

Fig. 12. Car–caravan combination with brake controller

The system has two operation modes:

Mode #1: In this mode the controller is working autonomously, independent of the driver's intention. When the combination of the vehicle state variables exceeds a predetermined (or adaptive) limit and the vehicle's motion starts to be irregular (spinning out, tends to jackknife, etc.) the controller automatically applies the appropriate side brake on both axles at passenger car, and on the rear axle on heavy commercial vehicles. The generated moment stabilizes the vehicle's motion.

Mode #2: This mode operates when the vehicle is being braked. The system is also able to release the brakes on the appropriate side. In this mode the controller coordinates the brake forces and produces stabilizing torque.

Fig. 13 shows the behaviour of a car–caravan combination (a) without any control, (b) with ABS only, (c) with ABS+SEC, (d) ABS+4WS. As seen, the ABS+SEC provides the best stability during this combined braking and turning manoeuvre (braking from 65 km/h on a road surface with $\mu = 0.4$) *Fig. 14* depicts the same four vehicles at μ-split test (the left hand side is $\mu = 0.9$, the right side is $\mu = 0.3$, braking from 80 km/h). The ABS–SEC vehicle goes on a straight line, the other three spin out in different extent.

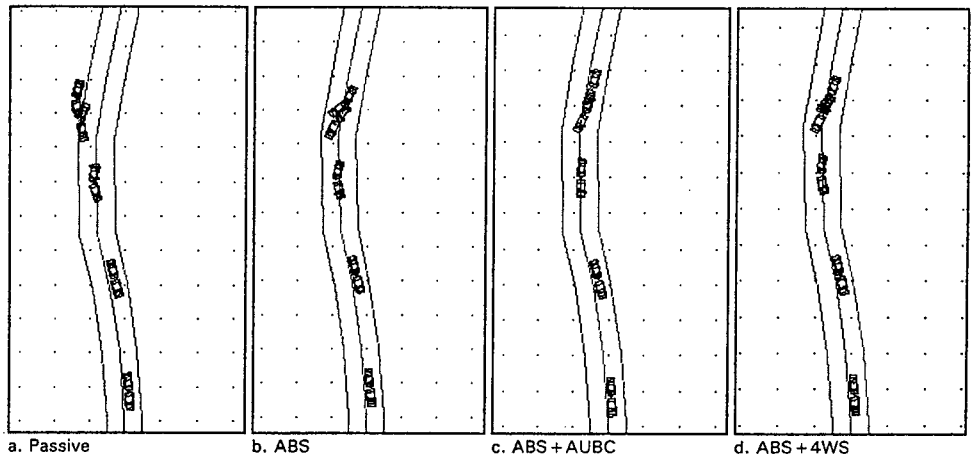

Fig. 13. Top views of the combined braking and turning manoeuvre

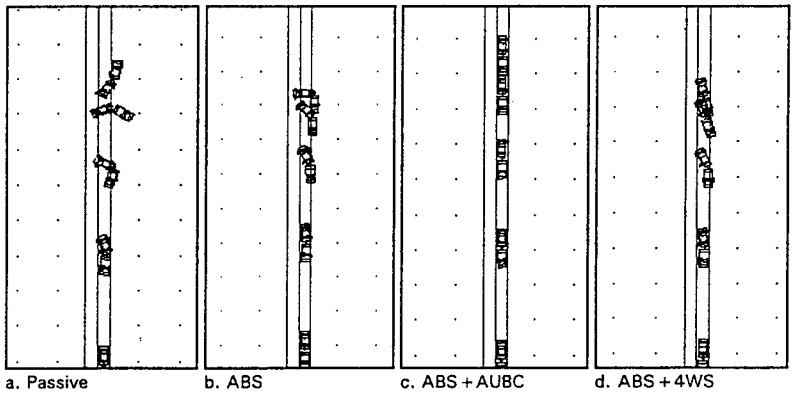

Fig. 14. Hard copies of the μ-split manoeuvres

5. Summary

In this state-of-art report the research activity of the Systems and Control Laboratory of the Computer and Automation Institute of the Hungarian Academy of Sciences and the Department of Road Vehicles, TUB conducted in the field of controlled vehicle dynamics. In the present state of the research the on-vehicle systems are emphasized, but the first steps are already done in the direction of the investigations into intelligent highway-vehicle systems as well.

Acknowledgement

The research projects targeting on the vehicle dynamical investigations were supported by the following research grants: Hungarian National Science Foundation (OTKA) grant No. F-015505 and T-016418.

References

[1] GIANONE, L. – PALKOVICS, L. – BOKOR, J. (1995): Design of an Active 4WS system with Physical Uncertainties, *Control Application*, (to be published).

[2] AMIROUCHE, F. – PALKOVICS, L. – WOODROOFFE, J. (1995): Optimal Driver Seat Suspension Design for Heavy Trucks, *Int. J. of Vehicle Design, Heavy Vehicle Systems*, (to be published).

[3] PALKOVICS, L. – EL-GLINDY, M. (1995): Design of an Active Unilateral Brake Control System for Five-Axle Tractor-Semitrailer Based on Sensitivity Analysis, *Vehicle System Dynamics*, Vol. 24, pp. 725–758.

[4] MICHELBERGER, P. – PALKOVICS, L. – BOKOR, J. (1993): Robust Design of Active Suspension System, *Int. J. of Vehicle Design*, Vol. 14, No. 2/3, pp. 145–165.

[5] PALKOVICS, L. (1992): Effect of the Controller Parameters on the Steerability of the Four Wheel Steered Car, *Vehicle System Dynamics*, Vol. 21, pp. 109–128.

[6] PALKOVICS, L. (1992): Investigation on Stability and Possible Chaotic Motions in the Controlled Wheel Suspension System, *Vehicle System Dynamics*, Vol. 21, pp. 269–296.

[7] PALKOVICS, L. – MICHELBERGER, P. – BOKOR, J. – GÁSPÁR, P. (1995): Adaptive Identification for Heavy-Truck Stability Control, *14th IAVSD Symposium*, Ann Arbor, MI, August 21–25.

[8] PALKOVICS, L. – BOKOR, J. – VÁRLAKI, P. (1995): Robust Controller Design for Active Unilateral Brake Control System, *European Control Conference, ECC'95*, Rome.

[9] PALKOVICS, L. – BOKOR, J. (1994): Stabilization of a Car-Caravan Combination Using Active Unilateral Brake Control, *AVEC'94, Int. Symposium on Advanced Vehicle Control*, October 24–28, Tsukuba, Japan, pp. 141–147.

[10] PALKOVICS, L. – SEMSEY, A. – AMIROUCHE, F. (1994): Vibration Control and Stability of the Pilot Head and Neck in Combat Helicopters, *Proc. of ASME'94 WAM*, December, 1994, Chicago, Illinois, USA – invited lecture.

[11] PALKOVICS, L. – VENHOVENS, P. – BOKOR, J. (1994): Design Problems of the Semi-Active Wheel Suspension System and a Possible Way of Their Elimination, *FISITA'94 World Congress*, China World Hotel, 17–21 October, 1994, pp. 11–16.

[12] BOKOR, J. – KERESZTES, A. – PALKOVICS, L. – VÁRLAKI, P. (1994): Design of an Active Suspension System in the Presence of Physical Parameter Uncertainties, *FISITA'94 World Congress*, China World Hotel, 17–21 October, 1994, pp. 30–41.

[13] PALKOVICS, L. – EL-GINDY, M. – ILOSVAI, L. (1993): Examination of Different Control Strategies of Heavy-Vehicle Performance, *1993 ASME WAM*, New Orleans, Lousiana, November 1993, DSC-Vol. 52, pp. 349–362.

[14] PALKOVICS, L. – GÁSPÁR, P. – BOKOR, J. (1993): Design of Active Suspension System in the Presence of Physical Parametric Uncertainties, *Proc. of ACC'93*, San Francisco, California, June 1993, USA., pp. 696–700.

[15] PALKOVICS, L. – BOKOR, J. – MICHELBERGER, P. – VÁRLAKI, P. – GIANONE, L. (1993): Robust Design of an Active 4WS System Using H_∞ and RLQR Approach, *Second European Control Conference ECC'93*, Groningen, July, 1993.

INFORMATION FOR AUTHORS

Submitting a Manuscript for Publication. Submission of a paper to this journal implies that it represents original work previously not published elsewhere, and that it is not being considered elsewhere for publication. If accepted for publication, the copyright is passed to the publisher: the paper must not be published elsewhere in the same form, in any language, without written consent of the executive editor. The first author will receive 50 free reprints.

Manuscripts should be submitted in English in two copies to the editors' office (see inner front cover). Good office duplicated copies of the text are acceptable.

Periodica Polytechnica is typeset using the TEX program with the AMSTEX macro package. Therefore, authors are encouraged to submit their contribution after acceptance in this form too, or at least the text of the article in a simple ASCII file (e. g. via email or on a floppy diskette, readable on an IBM compatible PC). By this solution most of the typesetting errors can be avoided, and publishing time can be reduced. An AMSTEX style file with a sample TEX source file is also available upon request.

Compilation and Typing of Manuscripts. Contributions should be typed or printed in double spacing (24 pt spacing when using text processors), on A4 paper. One page may contain not more than 10 corrections (paints do not count).

The maximum length of the manuscript is 30 standard pages (25 lines, with 50 characters in a line), including illustrations and tables. When more characters are typed on a page, the allowed page number is reduced accordingly.

When using a text processor, please use a (preferably English) spelling checker before the final printing.

Use one side of the sheet only. Paragraphs are to be indented by 5 spaces and not to be preceded by a blank line.

A correctly compiled manuscript should contain the following items:

(1) Title page giving: the suggested running header (max. 50 characters) for the odd typeset pages; the title (short, with subheading if necessary); the name(s) of the author(s); affiliation (institution, firm etc.) of the author(s), in English, with mailing address, telefax and phone numbers and email address; grants, scholarships etc. during the research (in a footnote); an informative abstract of not more than 200 words with 3-5 keywords;
(2) Textual part of the contribution with a list of references;
(3) A separate sheet listing all figure captions and table headers;
(4) Illustrations and tables (please put your name on each sheet), at least one set of illustrations in very good quality for reproduction.

Abstract. A summary or abstract of about 100-200 words should be provided on the title page. This should be readable without reference to the article or to the list of references, and should indicate the scope of the contribution, including the main conclusions and essential original content.

Keywords are to be given for the purpose of data bases and abstracting; avoid too general keywords which provide no help in literature searching.

General rules for the text. Chapters are to be numbered with Arabic numbers in decimal hierarchy.

Wherever possible, mathematical equations should be typewritten, with subscripts and superscripts clearly shown. Metric (SI) units are to be used, other units may be given in parentheses. Equations must be numbered on the right side, in parentheses. Handwritten or rare mathematical, Greek and other symbols should be identified or even explained if necessary in the margin. Letters denoting quantities are to be distinguished by different setting both in the formulae and in the text. Remember the rule that scalar quantities are to be denoted by italics (underline by hand in your manuscript), vectors by lower case bold type letters (underline doubled), and matrices by bold capitals (underline doubled). Dimensions (like cm, Ohm, V etc.) and standard function names (sin, ln, P etc.) are to be typeset in Roman typefaces (not in italics). A few important words may be distinguished by italic setting (underline).

Illustrations and Tables. Graphs, charts and other line illustrations should be drawn neatly in Indian ink, or printed by a laser printer. Computer printouts can only be used if they are of excellent quality. Figures should be submitted in an adequate size for camera-ready pages in size 1.2:1. Suggested line thicknesses: 0.18–0.35–0.4 mm or 0.5–0.7–1.14 pt. Letter sizes: 0.4 mm (10 pt). All figures should be numbered with consecutive Arabic numbers, have descriptive captions, and be referred to in the text. Captions should be self-explanatory, not merely labels. Figures must not contain lengthy texts; use captions instead.

Number tables consecutively with Arabic numbers and give each a descriptive caption at the top. If possible avoid vertical rules in tables. Tables should be preferably submitted in camera-ready form.

The earliest acceptable position of figures and tables is to be indicated in the left margin.

References. In the text references should be made by the author's surname and year of publication in parentheses, e.g. (Earl et al, 1988) or ...was given by Kiss and Small (1986a). Where more than one publication by an author in one year is referred to, the year should be followed by a suffix letter (1986a, 1986b etc.), the same suffix being given in the reference list. For the style of the reference list, which is to be given in alphabetical order, see the examples below for journal articles, conference papers and books.

Earl, J., Kis, I. and Török, I. (1988): Partial Discharge Measurement in Cables. *Periodica Polytechnica Ser. Electrical Engineering*, Vol. 32, No. 4, pp. 133–138.

Kiss, S. and Small, A. B. (1986a): Roundoff Errors in FFT. *Proc. 5th IEEE Symposium on Signal Processing*, Boston (MA), May 3–5, 1986. New York, NY, IEEE Press, CH0092-2875/86, pp. 3.5–3.9.

Kiss, S. and Small, A. B. (1986b): Ellenállások (Resistances). Budapest, Tankönyvkiadó. pp. 533–535. (in Hungarian)

More detailed guidelines for authors, with hints for the preparation of figures and with a sample page, are available from the editors' office (see inner front cover).

CONTENTS

ROHÁCS, J.: Theory of Anomalies and its Application to Aircraft Control 3

GAUSZ, T.: Aerodynamic Parameter Estimation of the CG Controlled Airplanes 19

SÁNTA, I.: Changes in Gas Turbine Maps as Results of Divergence in Geometrical Parameters 29

BÖHM, F.: From Non-Holonomic Constraint Equation to Exact Transport Algorithm for Rolling Contact 47

BOKOR, J. – PALKOVICS, L.: Modern Control Theory Applied to Vehicle Dynamic 65